

CrystEngComm

Accepted Manuscript



This is an *Accepted Manuscript*, which has been through the Royal Society of Chemistry peer review process and has been accepted for publication.

Accepted Manuscripts are published online shortly after acceptance, before technical editing, formatting and proof reading. Using this free service, authors can make their results available to the community, in citable form, before we publish the edited article. We will replace this *Accepted Manuscript* with the edited and formatted *Advance Article* as soon as it is available.

You can find more information about *Accepted Manuscripts* in the [Information for Authors](#).

Please note that technical editing may introduce minor changes to the text and/or graphics, which may alter content. The journal's standard [Terms & Conditions](#) and the [Ethical guidelines](#) still apply. In no event shall the Royal Society of Chemistry be held responsible for any errors or omissions in this *Accepted Manuscript* or any consequences arising from the use of any information it contains.

1

The Solid State, Surface and Morphological Properties of *p*-Aminobenzoic Acid in terms of the Strength and Directionality of its Intermolecular Synthons

I. Rosbottom and K.J. Roberts

*Institute of Particle Science and Engineering Institute for Process, Research and Development,
School of Chemical and Process Engineering, University of Leeds, Woodhouse Lane, Leeds, LS2 9JT*

R. Docherty

*Pfizer Global Research & Development, Pharmaceutical R & D (i.p.c 612), Sandwich, Kent
CT13 9NJ*

1 Keywords: Organic Crystallisation, Molecular Modelling, Morphology Prediction, Solution Crystal
2 Growth, Synthonic Engineering, Lattice Energy, Intermolecular Interactions, Atom-Atom Method,
3 Surface Chemistry, *p*-Amino Benzoic Acid

4

5

6

7

8

9

10

11

12

13

14

2

1 **Abstract:**

2 Empirical forcefield calculations utilising the atom-atom method were used to examine the strength,
3 directionality and chemical state of the intermolecular interactions (synthons) present in the polymorphic forms
4 (α and β) of *p*-aminobenzoic acid (*p*ABA). This is set within the context of predicting the morphology of both
5 forms in terms of the unsatisfied synthons at each growth surface. The α lattice energy was calculated to be -
6 24.54kcal/mol with the dominant intermolecular interactions found to consist of OH...O carboxylic acid H-
7 bonding dimers and head to head π - π stacking interactions. The β lattice energy was calculated to be -
8 22.73kcal/mol and the dominant interactions found to consist of a 4-membered H-bonding ring made up of two
9 identical NH...O and OH...N interactions, plus strong head to tail π - π stacking interactions. The NH₂ group was
10 calculated to contribute more to the β lattice energy than to the α , as it acts as a H-bonding donor and acceptor in
11 the β structure, whilst acting solely as a donor in α . Conversely, the COOH group was found to contribute more
12 strongly to the α lattice energy due to the formation of the OH...O H-bonds and also NH...O H-bonds, while
13 the COOH group in the β structure forms only weaker O...HN and OH...N interactions. Morphological
14 prediction of the β form gave greater resemblance to the experimental morphology compared to α . Surface
15 chemistry analysis revealed that the strength, character and directionality of the synthons present varies in terms
16 of their anisotropy between these two polymorphs. The strength and character of the unsaturated synthons
17 exposed at the major surfaces of the α crystal were found to significantly vary, which results in a needle-like
18 morphology. In contrast, the strength and character of the synthons exposed at the major surfaces of the β
19 morphology were found to be much more similar, which results in the more equant morphology. Overall, this
20 paper presents a synthonic, analytical approach which holistically links the molecular properties with the bulk
21 and surface synthons, and through this rationalises their contributions to the growth and morphology of this
22 organic crystalline system.

23

24

25

26

27

3

1	Table of Contents
2	1. Introduction
3	2. Synthonic Modelling
4	2.1. Bulk Intrinsic Synthons
5	2.2. Surface Extrinsic Synthons
6	3. Materials
7	3.1. Materials
8	3.2. Computational Methods
9	3.2.1. Structure Minimisation
10	3.2.2. Lattice and Attachment Energy Calculations
11	3.2.3 Analysis of the Cambridge Structural Database
12	3.3. Experimental Methods
13	3.3.1 Growth of Crystals
14	3.3.2 Optical Goniometry
15	4. Results and Discussion
16	4.1. Conformational Analysis
17	4.2. Lattice Energy Calculations
18	4.3. Bulk Intrinsic Synthons
19	4.4. CSD Analysis of Important H-bonding Interactions
20	4.5. Morphological Simulations and Surface Chemistry Analysis
21	4.5.1. Attachment Energy Morphology Analysis
22	4.5.2. Confrontation of Morphological Simulation to Experimental Data
23	4.5.2.1. α -form
24	4.5.2.2. β -form
25	4.5.3. Surface Chemistry Analysis
26	4.5.3.1. α -form
27	4.5.3.2. β -form
28	4.5.4. Comparison between α and β Morphologies

4

1 5. Conclusions

2 **Nomenclature**

3 BFDH: Bravais, Friedel, Donnay, Harker.

4 PBC: Periodic Bond Chains

5 vdW: van der Waals

6 H-Bonding: Hydrogen Bonding

7 CSD: Cambridge Structural Database

8 BCF: Burton Carbera and Frank

9 B & S: Birth and Spread

10 RIG: Rough Interfacial Growth

11 3D: 3 dimensions

12

13 **List of Symbols**14 E_{cr} : Lattice Energy15 E_{sl} : Slice Energy16 E_{att} : Attachment Energy17 ΔH_s : Sublimation Enthalpy

18 R: Gas Constant

19 T: Temperature

20 ξ : Anisotropy Factor21 \underline{n} : Growth Direction22 $\otimes \underline{n}$: Growth Direction Perpendicular to Plane of the Page

1 1. Introduction

2 The study of crystal surfaces from a structural perspective can be a powerful tool in predicting the
3 optimum conditions for solution crystallisation. Understanding and controlling the shape of crystals
4 can be a critical quality attribute in terms of enabling an active ingredient to be processed to a viable
5 product¹. Morphology prediction and screening is therefore very important for industry to obtain
6 desirable crystalline shapes for filtering and downstream processing. These predictions can further the
7 knowledge of the growth mechanisms of a crystal surface and through this direct the final morphology
8 of a crystalline particle. In addition, knowledge of the surface chemistry of crystals, as derived from
9 morphological simulation, can provide a vital insight into the materials crystal/crystal aggregation
10 properties and hence their formulation²⁻⁴.

11 Early relationships of interplanar spacing to morphological importance, linked with lattice geometry,
12 lead to the Bravais, Friedel, Donnay and Harker model (BFDH)⁵⁻⁹. This model is still used to identify
13 the morphologically dominant faces (hkl). However, this model neglects the chemistry of the
14 interactions present within the crystal, which for a molecular crystal are often dominated by isotropic
15 van der Waals (vdW) interactions coupled with more directive hydrogen bonds (H-bonds). In
16 particular, the BFDH approach doesn't effectively deal with these directional H-bonding interactions,
17 and this has been demonstrated in the prediction of the morphology of β -succinic acid¹⁰.

18 In 1954, Hartmann and Perdok¹¹ expanded Born's assumption that surface energy is directly related to
19 chemical bond energies¹² through the periodic bond chain (PBC) theory and introduced the term
20 'attachment energy' (E_{ATT}). PBC's are strong stoichiometric intermolecular interactions that run in-
21 plane with respect to a growing face and any face containing at least two of these can be assumed to
22 facilitate stable, slow growth and therefore be present at the surface of an experimentally grown
23 crystal¹¹. In turn, it is then assumed that the faces with a low attachment energy grow slowly and are
24 therefore morphologically important. This idea was expanded for inorganic materials by Dowty with
25 the use of the term 'template fraction', which describes the fraction of energy holding growth layers to
26 substrates¹³. Hartmann and Bennema showed that assuming the relative attachment energies are

6

1 proportional to relative face specific crystal growth rates is a valid approximation for faces growing
2 by either a Burton, Carbera and Frank (BCF) mechanism¹⁴ or birth and spread mechanism¹⁵ below the
3 roughening transition temperature¹⁶, and a robust method for deriving the morphology of molecular
4 crystals from their internal structure and symmetry was demonstrated by Berkovich-Yellin¹⁷. Building
5 on this, computational methods for the routine prediction of the strength, directivity and dispersive
6 nature of intermolecular interactions, together with their summation for predicting crystal lattice and
7 surface attachment energies for morphological prediction were developed through the HABIT
8 programme¹⁸ by Roberts and co-workers¹⁹. In parallel to this, within the crystallographic, solid-state
9 and supra-molecular chemistry community, the importance of hydrogen bonding interactions and
10 graph theory^{20, 21} was recognised, in particular their potential importance for understanding
11 polymorphism²² and for crystal engineering the design of materials²³. More recently, the concepts as
12 to how the shape of molecules, together with the directionality and strength of their interactions, can
13 strongly influence the physical properties of crystalline materials have been reviewed by Desiraju²⁴.

14 The attachment energy model relies, to some extent, on the interactions between the molecules
15 interacting at the crystal surface and the solution being almost the same as the bulk interactions of the
16 crystal, and this proportionality concept has been proved to be a good approximation for a variety of
17 studies^{18, 25-27}. Calculating the relative strength of the intermolecular interactions using atomistic
18 force-fields derived from empirical data, through the atom-atom method²⁸, can provide good
19 prediction of the physical properties of molecular crystals²⁹⁻³³. However, more recent publications
20 highlighted the option to optimise these potentials against *ab initio* data and crystal structures to create
21 an interatomic interaction potential which is specific to each crystalline system³⁴⁻³⁶.

22 The most significant draw back of the attachment energy model is that it fails to take into account
23 external conditions such as temperature and surrounding solvent interactions with a crystal surface.
24 More recent models attempt to account for the effect as to how a surface de-solvates prior to solute
25 incorporation by calculating solvent binding energies and applying models that considers the size of
26 the surface and the concentration of the solution³⁷⁻³⁹. Further models have also attempted to predict

7

1 the effect of different growth mechanisms on the attachment energy of a given surface⁴⁰, but these
2 models have yet to be proven effective over a required number of crystalline systems and
3 environments. Molecular dynamics simulations can provide valuable information in predicting the
4 solvent adsorption at a surface and how this affects crystal growth⁴¹⁻⁴³ but the downside of this
5 approach is that these calculations are often time consuming and require a high amount of molecular
6 modelling expertise.

7 In this study, a holistic method is presented, which can be relatively easily reproduced by less
8 specialised computational scientists, for examining crystal morphology by analysing the molecular,
9 crystal structure and morphological properties of a model organic system, i.e. the α and β forms of *p*-
10 amino benzoic acid (*p*ABA). To achieve this, the conformational space of the molecule and the
11 intermolecular hydrogen bonding lengths are compared to similar crystal structures present in the
12 Cambridge Structural Database (CSD)⁴⁴. The lattice energies are calculated and the individual atom
13 and functional group contributions to the lattice energy are compared between the α and β
14 polymorphs. The bulk intermolecular interaction strengths are calculated and ranked, and the
15 dominating interatomic interaction type established. The morphology of the two polymorphs is
16 predicted assuming monomer attachment to each crystal surface. In addition, the morphology of α is
17 predicted assuming a carboxylic acid dimer is the attaching crystal growth unit. Finally, the surface
18 chemistry of both forms is analysed by establishing the key intermolecular interactions that contribute
19 to the attachment energies of the morphologically important surfaces. This is summarised in scheme
20 1:

21

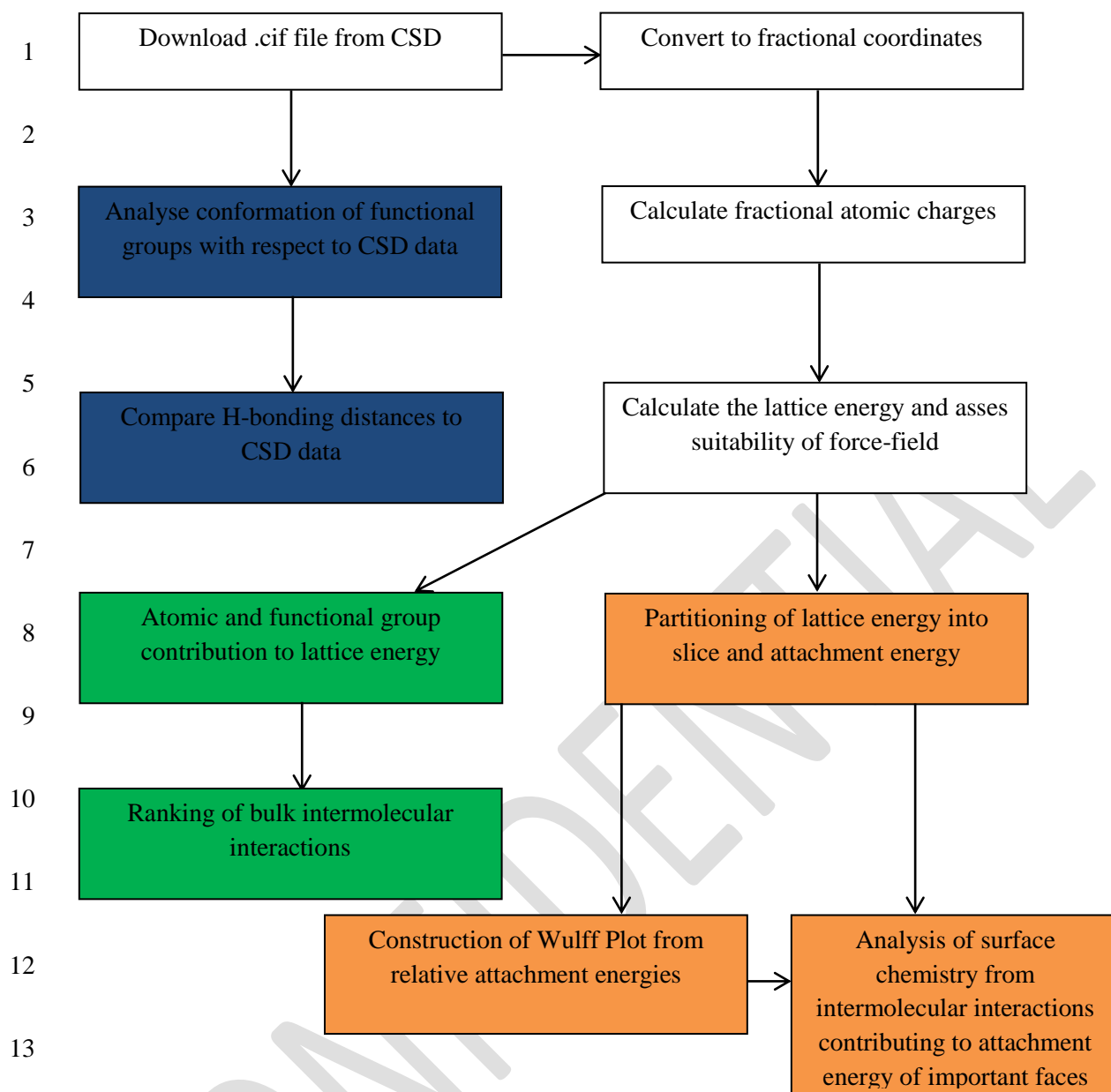
22

23

24

25

8



15 **Scheme 1: Flow diagram of how the data was obtained for each stage of the morphological**
16 **analysis. Structure file preparation, charge and initial calculations shown in white. CSD data**
17 **analysis shown in blue. Bulk intermolecular interaction data shown in green. Surface and**
18 **morphological data shown in yellow.**

19

20

21

1 **2. Synthonic Modelling**

2 Synthonic Modelling draws upon the molecular and crystallographic structure of a material and
3 involves the calculation of the strength, directionality and chemical state associated with pairwise
4 intermolecular interactions (synthons) within a crystal structure using the atom-atom approach⁴⁵. This
5 information can be used to predict physical and chemical properties of the crystal such as shape,
6 cluster stability, mechanical properties etc.

7 **2.1. Bulk Intrinsic Synthons**

8 Summation of intermolecular interactions can be used to calculate a molar lattice energy. The
9 intermolecular interactions can be ranked by strength or distance and outputted for analysis, along
10 with the atom by atom contribution to the lattice energy summed over the asymmetric unit. Further
11 analysis of the lattice energy as a function of limiting radius can be utilised to reveal information on
12 the initial coordination sphere of a crystal structure involved in nucleation and the early stages of the
13 growth process. In turn, this reveals the intermolecular interactions that need to be saturated in the
14 bulk crystal chemistry for lattice energy convergence. The bulk saturated intermolecular interactions
15 can be referred to as ‘intrinsic synthons’.

16 **2.2. Surface Extrinsic Synthons**

17 The lattice energy can be partitioned into slice and attachment energy per surface as defined by
18 specified Miller planes (*hkl*). The magnitude of the attachment energy per face can be taken to predict
19 the relative growth rate and hence morphological importance of the surface. Face-specific
20 information, such as which of the bulk intrinsic synthons are unsaturated (broken) due to surface
21 termination can be outputted for analysis. These unsaturated interactions are known as ‘extrinsic
22 synthons’. The nature and strength of these interactions, combined with molecular scale modelling of
23 the predicted surfaces using molecular visualisation software, can be used to reveal detailed
24 information on the surface chemistry of the important faces and how e.g. the solute and solvent
25 molecules potentially bind and incorporate into the lattice. This information can then be directly
26 related to the relative growth rate and size of the crystal face.

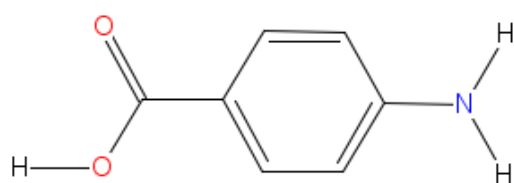
10

1 3. Materials and Methods

2 3.1. Materials

3 This study focusses on the α and β forms of *p*ABA. The crystal structures of these forms
4 (AMBNAC01 and AMBNAC06) are taken from the CSD⁴⁴.

5 The molecular structure of *p*ABA consists of a phenyl ring with a carboxylic acid group and amino
6 group in the para position.

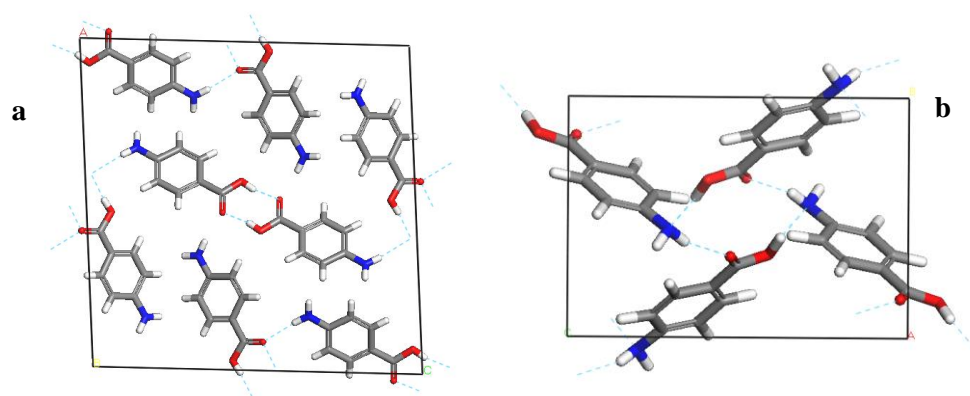


7

8 **Figure 1: The molecular structure of *p*ABA. Functionality consists of three hydrogen bonding**
9 **donors (amino hydrogens and carboxylic acid hydrogen) and three hydrogen bonding acceptors**
10 **(amino nitrogen and carboxylic acid oxygens).**

11 *p*ABA is known to crystallise in two well-characterised polymorphs, α ⁴⁶ and β ⁴⁷. A recent study has
12 revealed a third polymorph, this has an orthorhombic crystal structure, which was found by
13 crystallising from aqueous solutions containing *p*ABA and selenous acid⁴⁸, but this latter structure
14 was not considered here. Both the α and β crystal structures are monoclinic with a $P2_1/n$ space group.
15 The α form crystallises with two molecules in the asymmetric unit and eight molecules in the unit cell
16 with dimensions $a = 18.55\text{\AA}$, $b = 3.86\text{\AA}$, $c = 18.64\text{\AA}$ and $\beta = 93.56^\circ$. The β form crystallises with one
17 molecule in the asymmetric unit and four molecules in the unit cell with dimensions $a = 6.27\text{\AA}$, $b =$
18 8.58\AA , $c = 12.36\text{\AA}$ and $\beta = 100.13^\circ$.

11



1
2 **Figure 2: Details of unit cells of α -*p*ABA (a) and β -*p*ABA (b) displaying their associated packing**
3 **motifs. α packing consists of COOH...HOOC H-bonding dimers and NH...O H-bonds. β packing**
4 **consists of a 4 membered H-bonding ring with identical OH...N and NH...O interactions.**

5 Figure 2a shows that the packing of the α form is found to be dominated by the formation of non-
6 equivalent OH...O H-bonding dimers between neighbouring carboxylic acid groups. In addition, the
7 *p*ABA molecules are found to form a head to head stacking motif in the b direction creating π - π
8 stacking interactions. Figure 2b shows that the packing of the β form is found to be dominated by a 4
9 membered H-bonding ring motif consisting of alternating OH...N and NH...O H-bonds. In addition,
10 the *p*ABA molecules are also found to form head to tail stacking motifs creating π - π stacking
11 interactions.

12 The α form of *p*ABA is observed to crystallise in a needle-like morphology, while the β form has a
13 more equant morphology⁴⁹. The α morphology is of particular significance due to the associated
14 issues with controlling the chemical process behaviour of needle-like crystals in pharmaceutical and
15 fine chemical industries. Hence, there is a desire to control the shape of crystalline particles and recent
16 studies have highlighted the challenge of predicting and experimentally controlling the morphology of
17 needle-like crystals^{39, 50, 51}. Therefore there is a clear need to better understand the growth of these
18 crystals from a molecular standpoint.

19 3.2. Computational Methods

20 3.2.1 Structure Minimisation

12

1 The crystal structures were minimised using the Forcite module in Materials Studio⁵² keeping the
2 molecules rigid and the unit cell parameters constant. The SMART algorithm was selected for the
3 structural minimisation. The DREIDING forcefield³¹ was used as this was the most suitable forcefield
4 available in Materials Studio for treating organic molecules.

5 **3.2.2: Structure File Preparation**

6 The .cif file for each crystal structure was obtained from Mercury 3.3⁵³. The .cif file was imported
7 into Materials Studio, the unit cell of the crystal was built to apply the symmetry and the structure was
8 then exported as a .car file (Cartesian coordinates). The Cartesian coordinates were then converted
9 into fractional coordinates.

10 **3.2.3 Lattice and Attachment Energy Calculations**

11 HABIT^{18, 54} was used for the calculation of the pairwise intermolecular interaction strengths and
12 lattice energy. HABIT takes structural information and constructs a series of unit cells in three
13 dimensions. From a molecule in the origin cell, the non-bonded energy between it and all other
14 molecules in the other unit cells are calculated within a user-defined radius. The breakdown of lattice
15 energy per molecule, atom type and functional group was achieved using the DEBUG-2 function. For
16 the purposes of molecular analysis, *p*ABA was sub-divided into three molecular components: amino,
17 phenyl and carboxylic acid. The functional group contributions to the lattice energy reflect the
18 summation of the individual contribution of the atoms involved within each component. The
19 contributions per functional group and per atom type were summed over the asymmetric unit. The
20 ranking of the intermolecular interactions by strength was outputted using the DEBUG-1 function.
21 The α form has two molecules in the asymmetric unit ($\alpha 1$ and $\alpha 2$) and the lattice energy was averaged
22 over the summations with respect to the two molecules. Therefore the ranking of intermolecular
23 interactions had to be partitioned between $\alpha 1$ and $\alpha 2$. These calculations were initially based on a
24 monomer growth unit, and then on the basis of carboxylic acid H-bonding dimer growth unit.

25 The intermolecular interactions were calculated using the Momany force-field²⁹ containing a Lennard-
26 Jones potential for the vdW interactions, a specific 10-12 H-bonding potential and a Coulombic term

1 with respect to the electrostatic interactions. This force-field has previously shown good correlation of
2 calculated and experimental lattice energies of crystalline materials containing both H-bonding and π -
3 orbital functionality^{5, 10, 55}.

4 For the calculations of the electrostatic interactions, the Restrained Electrostatic Potential (RESP)
5 charges based on *ab initio* MP2/aug-cc-pvtz theory derived from the Antechamber within Ambertools
6 were calculated⁵⁶. The single molecule of *p*A₄ was optimized at the MP2/aug-cc-pvtz level and the
7 optimized structure's electrostatic potential was calculated with Gaussian09⁵⁷. The ESP data created
8 from Gaussian is converted into a RESP format in Antechamber and finally the RESP fit is applied
9 with Ambechamber to calculate the actual RESP charges.

10 From the intermolecular energy calculations, the lattice energy was calculated (E_{cr}). The suitability of
11 the potential was evaluated by comparison with the sublimation enthalpy (ΔH_s), given by equation 1:

$$E_{cr} = \Delta H_s - 2RT \text{ (Equation 1)}$$

12 The most likely growth slices were selected on the basis of the BFDH rule using MORANG⁹, stating
13 that the faces with the largest interplanar spacing (d_{hkl}) are likely to be morphologically important at
14 the surface⁵. For the slices with the largest interplanar spacing, the lattice energy (E_{cr}) was partitioned
15 into slice energy (E_{sl}) and attachment energy (E_{att}), according to equation 2¹⁷:

$$E_{cr} = E_{sl} + E_{att} \text{ (Equation 2)}$$

16 The relative attachment energies of each face were expressed as centre to face distances, then used to
17 create a Wulff plot to represent the external morphology using SHAPE^{53, 58}. In addition, the surface
18 anisotropy factor:^{59, 60}

$$\varepsilon_{hkl} = \frac{E_{hkl}^{sl}}{E_{cr}} \text{ (Equation 3)}$$

19 was calculated to provide a measure as to how satisfied the possible intermolecular interactions of a
20 molecule at a growing surface are when compared to those of a molecule within the bulk.

14

1 The nomenclature used to label the interactions identified the strongest interaction as capital A (i.e.
2 alphabetically), with α or β referring to the polymorphic form and 1 or 2 relating to the different
3 crystallographically independent molecules within the asymmetric unit (α -structure). The packing
4 diagrams were annotated to show some of the strongest interactions with two labels on, e.g. $D\alpha 1/D\alpha 2$,
5 indicates the intermolecular interactions between the two molecules within the asymmetric unit.

6 This basic nomenclature was also used to characterise the surface-specific interactions at a given
7 surface (hkl).

8 **3.2.4: Analysis of the Cambridge Structural Database**

9 Analysis of the molecular conformation within the crystal structures was undertaken using the CCDC
10 tools⁵³. Conquest 1.16⁵³ was used to define the fragments and torsion angles to search for in the CSD.
11 The NH_2 torsion angle was defined as the torsion between the plane of the phenyl ring carbons and
12 the hydrogens attached to the nitrogen, using a four body torsion C-C-N-H. Similarly, the COOH
13 torsion angle was defined as the torsion between the plane of the phenyl ring carbons and the two
14 oxygens on the COOH group, using a four body torsion C-C-C-O. The outputted results were
15 analysed using Mercury 3.3⁵³.

16

17 **3.3: Experimental Methods**

18 **3.3.1: Growth of Crystals**

19 Crystals of α -*p*ABA for comparison to simulation were prepared by spontaneous nucleation by slow
20 solvent evaporation from saturated ethanol solutions.

21 **3.3.2 Optical Goniometry**

22 The angles between the crystal faces of experimentally grown crystals were measured using a Huber
23 2-circle optical goniometer. The crystals were mounted so that the (0 1 0) zone of the crystal could be
24 viewed, and the crystal was rotated, noting the angle at which strong reflections of the light were

15

1 observed. In addition, for the morphological analysis, the expected interplanar angles were calculated
2 using Morang⁹.

3 **4. Results and Discussion**

4 Table 1 summarises the examination of the molecular structure, crystal chemistry, CSD analysis and
5 key intermolecular interactions, highlighting how they contribute to the lattice energy. The detailed
6 analysis of these results is presented in sections 4.1-4.4.

7

8

9

10

11

12

13

14

15

16

17

18

19

20

CONFIDENTIAL

16

- 1 **Table 1: Summary of crystallography, solid form data and lattice energy contributions for both**
 2 **polymorphs. This table collects much of the important data that is referred to in 4.1-4.4. Lattice**
 3 **energy contributions for both the monomer attachment and attachment of the carboxylic acid**
 4 **H-bonding dimer growth unit shown for α -pABA.**

α	Attribute	β
Crystallographic Data		
18.55	a (Å)	6.27
3.86	b (Å)	8.58
18.64	c (Å)	12.36
93.56	β (°)	100.13
P2 ₁ /n	Space Group	P2 ₁ /n
4, 2	Z, Z'	4, 1
1332.319 / 166.54	Cell / Molecular Volume (Å ³)	655.907 / 163.98
1.373	Density (g/Å ³)	1.389
Solid Form Informatics		
Pyramidal	NH ₂ Geometry	Pyramidal
OH...O dimers and NH...O	H-Bonding Network	OH...N and NH...O 4 membered ring
Head to head ~3.38	π - π Stacking Interaction (Å)	Head to Tail ~4.0
1.99 & 2.00	OH...O H-bonding Distance (Å)	N/A
N/A	OH...N H-bonding Distance (Å)	2.06
2.05	NH...O H-bonding Distance (Å)	2.19
Lattice Energy Contributions		

-24.51	Lattice Energy (kcal/mol)	-22.73
15.33%/16.8%	NH₂ (monomer attachment) / NH₂ (carboxylic acid dimer attachment)	23.8%
39.81%/59.9%	C₆H₄ (monomer attachment) / C₆H₄ (carboxylic acid dimer attachment)	42.5%
44.86%/23.3%	COOH (monomer attachment) / COOH(carboxylic acid dimer attachment)	33.7%
7	Number of Key Interactions (above 0.9kcal/mol)	8
71	Percentage of Lattice Energy from Key Interactions	75
30	Molecular Cluster Size for Lattice Energy Convergence	35

1 **4.1: Conformational analysis**

2 The torsion angles of the functional groups of published structures of both polymorphs are shown in
3 table 2:

4 **Table 2: Conformational Analysis of the COOH and NH₂ functional group torsion angles for**
5 **the published crystal structures in the CSD for *p*ABA α and β . Two values given for the α**
6 **structures as there are two molecules in the asymmetric unit.**

7

8

9

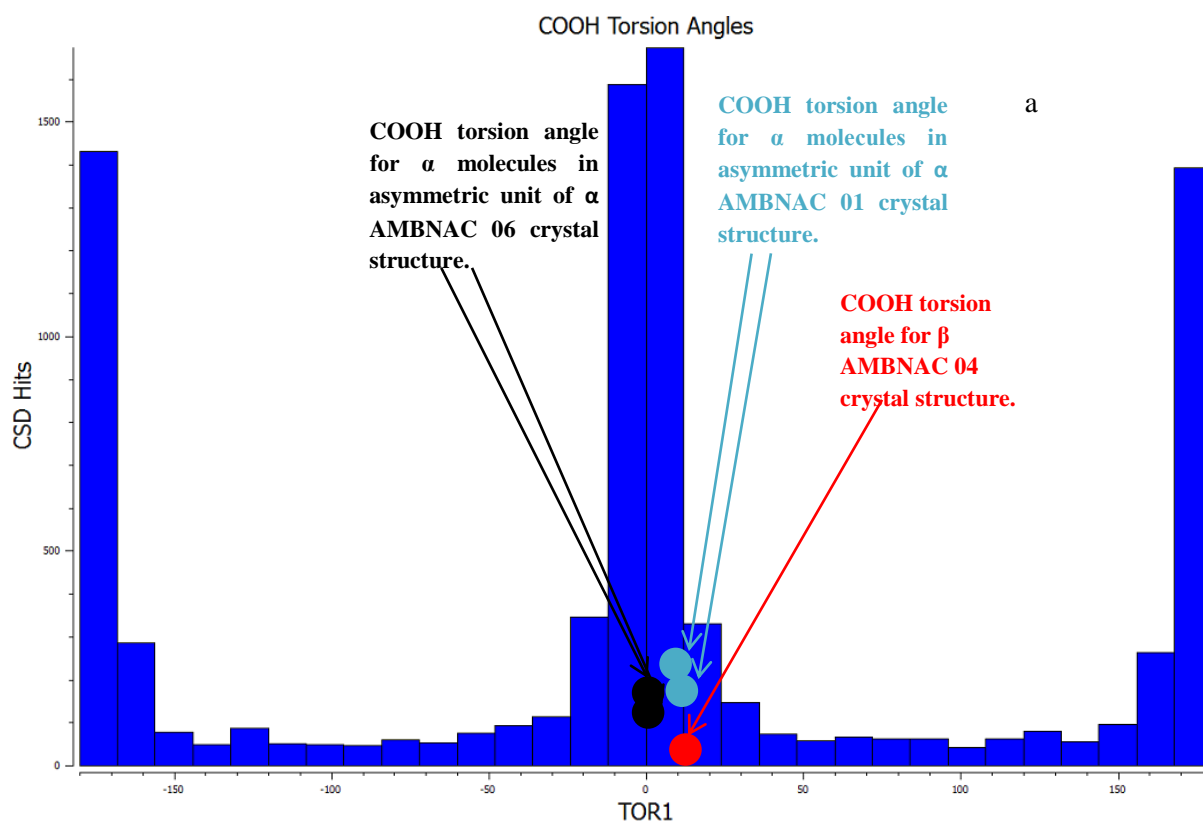
10

COOH Torsion Angle (°)	Polymorph	Ref Code	Lead Author	Year Published	C-C-N-H Torsion Angle (°)
2.865, 1.172	α	AMBNAC 01	Lai	1967	12.03, 11.17
0.866, 0.852	α	AMBNAC 06	Athimoolan	2007	0.024, 0.008
10.397	β	AMBNAC 04	Gracin	2005	26.844

1

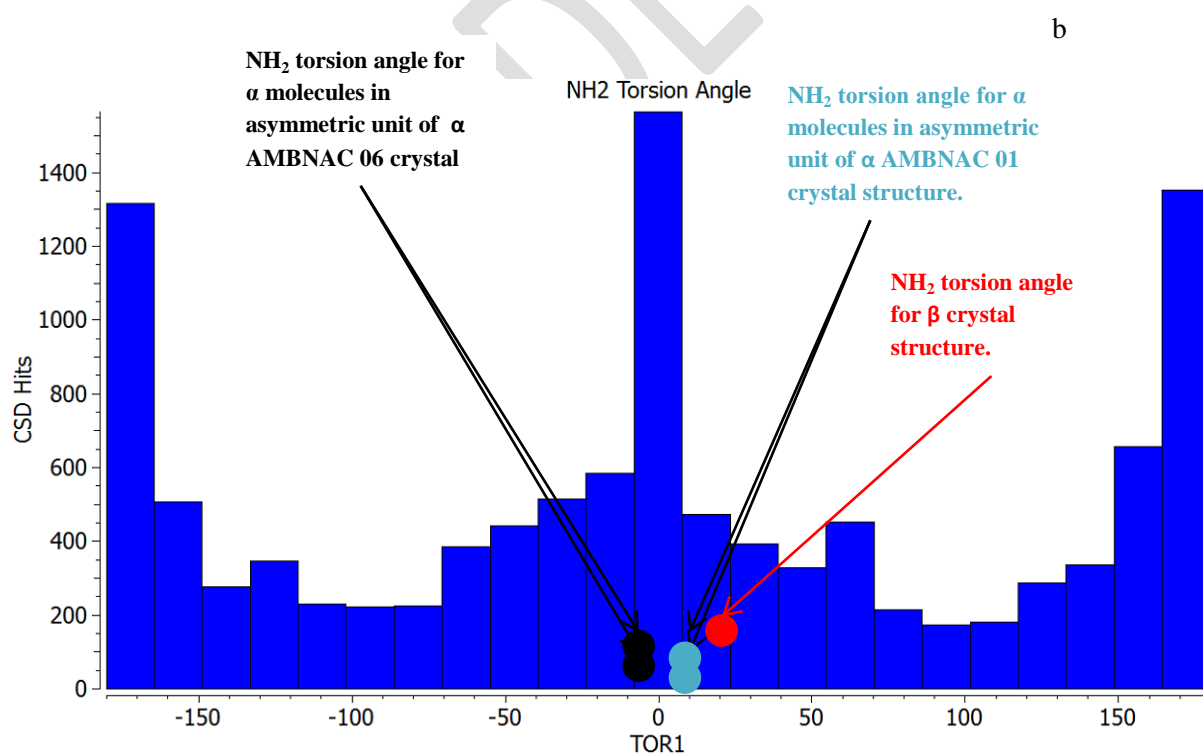
2 Table 2 shows the COOH group of the α structures were found to be almost completely planar with
3 respect to the phenyl ring, while the β structure was found to have a torsion angle of around 10°. The
4 formation of the OH...O H-bonding dimers that run planar to the phenyl ring appears to hold the
5 COOH planar with respect to the phenyl ring, while the NH...O and OH...N interactions in the β form
6 are not directed planar to the ring and hence the torsion angle is around 10° away from the plane of
7 the ring. Figure 3 reveals that the majority of crystal structures with a COOH group attached to a
8 phenyl ring in the CSD are close to planar.

9



1

2



3

4 **Figure 3a:** Torsion angles of COOH groups attached to a phenyl ring found in the CSD. Reveals

5 that vast majority of the groups are planar or very close to planar with respect to the phenyl

1 **ring. Figure 3b: Histogram of the amount of hits from the CSD as a function of torsion angles of**
2 **NH₂ hydrogens from the phenyl ring from planar to 45°. Majority of hits have a planar NH₂**
3 **similar to that of the AMBNAC06 α structure, spread of hits up to around 40° torsion broadly**
4 **similar.**

5 The conformation of the NH₂ group is of some interest as the two structures published in the CSD
6 have different conformations, the structure published by Lai in 1967 showing a torsion angle of
7 around 12° from the plane of the phenyl ring, while the more recent structure from Athimoolan
8 suggests that it is planar.

9 Figure 3b shows the majority of structures were found to have a close to planar NH₂. The spread of
10 hits at more pyramidal angles was found to be fairly level all the way up to 45°. Comparison of the
11 calculated lattice energies, ranking of intermolecular interactions and attachment energies showed
12 little difference between the planar and pyramidal structures for the major interactions of α -*p*ABA
13 (section S4, supplementary information). This analysis, together with recently published work by
14 *Schroeder et al*⁶¹ suggesting that the NH₂ in the α structure may be pyramidal, resulted in the crystal
15 structure with the pyramidal NH₂ group published by Lai et al (AMBNAC01) being chosen for this
16 study.

17 **4.2 Lattice Energy Calculations**

18 The lattice energy for each structure was calculated and compared to experimentally measured
19 sublimation enthalpies. The experimental lattice energy, as calculated from equation 4 and based on
20 published sublimation enthalpy data for α -*p*ABA was found to be between 26.77kcal/mol⁶² measured
21 at 373K using a torsion effusion method, and 27.25kcal/mol⁶³ also measured at 373K using a
22 calorimetric method. The calculated lattice energy for the α -form was found to provide a good match
23 to sublimation enthalpy data, hence suggesting that the Momany forcefield was a sensible choice for
24 calculating the strength of the intermolecular interactions within the crystal structures of *p*ABA. There
25 are no known published values for the sublimation enthalpies of β -*p*ABA.

21

1 Table 1 demonstrates how the intermolecular packing for each polymorph affects the respective
2 contribution of the functional groups to the lattice energy. In this, the NH₂ group was found to
3 contribute significantly more to the lattice energy of the β structure than α, as in the β structure the
4 NH₂ acts as a H-bonding donor and acceptor, while in the α structure the NH₂ acts only as a donor.
5 The strong H-bonds formed between the COOH groups in the α structure consequently give a larger
6 contribution from the COOH group in α than β. Table 1 also compares the functional group
7 contribution to the lattice energy of the α structure based on both monomeric and dimeric building
8 blocks. The loss of the intermolecular energy from the carboxylic acid group was found to result in
9 the major contributor to the lattice energy becoming the phenyl ring group, with the π-π stacking
10 interactions becoming, in terms of interaction energy, the most important synthons in the crystal
11 structure.

12

13

14

15

16

17

18

19

20

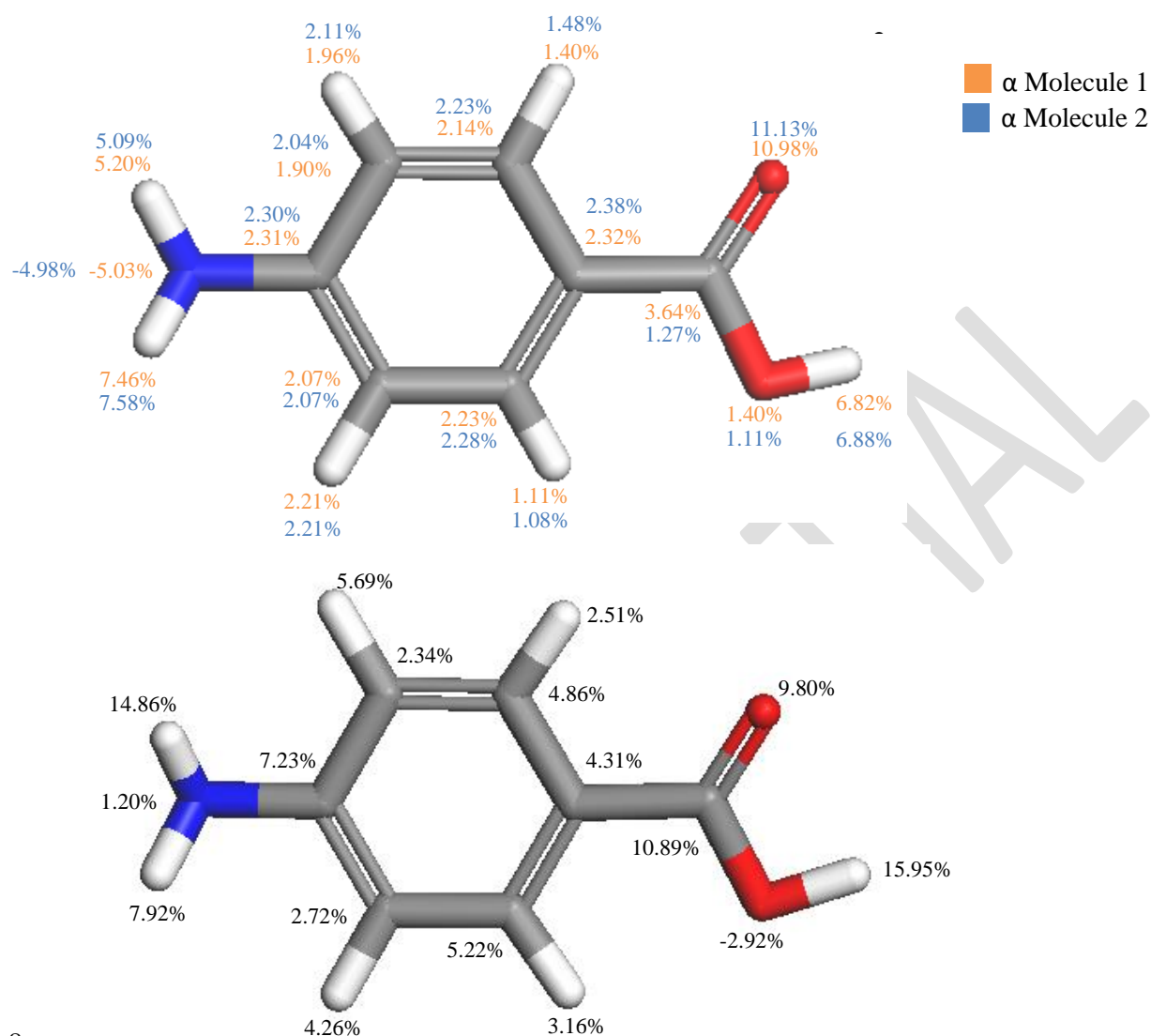
21

22

23

22

1 The individual atom-atom contributions to the lattice energy are given in figure 4:



8

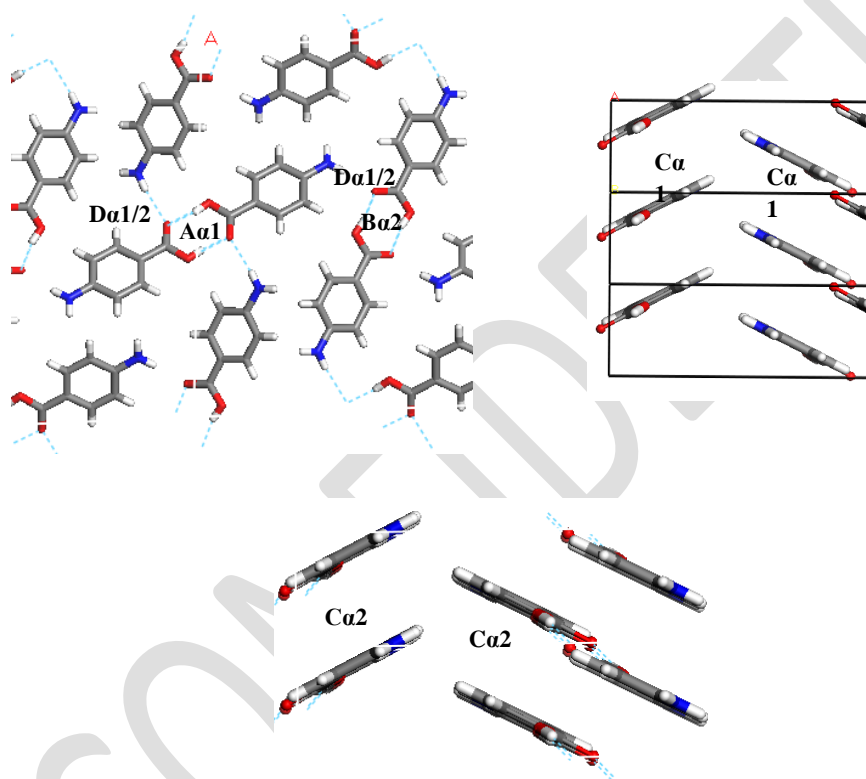
9 **Figure 4: Molecular structures of *p*ABA highlighting the percentage contribution of the lattice**
 10 **energy of α (top) and β (bottom) per atom. Contributions of the two molecules of α broadly**
 11 **similar due to the similar environments, whereas the β form shows increased importance of the**
 12 **amino hydrogens and hydroxyl hydrogen, and decrease in contribution from carbonyl oxygen.**
 13 **Reflects COOH dimer formation in α and NH₂ donor and acceptor capabilities in β .**

14 The atomistic contributions to the lattice energy from the asymmetric unit shown in figure 4 for both
 15 polymorphs reflect the intermolecular packing of both structures. The β form was found to show a
 16 significantly increased contribution from the amino nitrogen and hydrogens when compared to that
 17 for the α form, as the amino functional group acts as both a H-bonding donor and acceptor to form the

1 primary H-bonding synthons of the β structure. Conversely, it is interesting to note the significant
 2 increase in contribution from the hydroxyl hydrogen in the α form compared to that of the β structure.
 3 This reflects the much greater strength of the OH...O H-bonds compared to the OH...N H-bonds in β ,
 4 and how important they are in formation of the α crystal structure.

5 4.3: Bulk Intrinsic Synthons

6 To understand which interactions need to be saturated for lattice energy convergence, the strongest
 7 interactions in each polymorph were evaluated.



13

14

15

16

17

18 **Figure 5: Strongest interactions of α -*p*ABA labelled on the α packing diagram. Combination of**
 19 **H-bonding interactions (A, B and D) and π - π stacking (C) indicating that both types of**
 20 **interactions are important in the formation of α . Interactions tabulated table 3a and 3b.**

21 **Table 3: 7 strongest intermolecular interactions from α molecule 1(a) and 2 (b). A full list of the**
 22 **intermolecular interactions in the α structure is available in supplementary information.**

24

- 1 Distance (column 3) reflects centre of mass to centre of mass of the molecules involved in the
 2 interaction (herein and after).

a

Bond	Multiplicity	Distance (Å)	Intermolecular Energy (kcal/mol)	Percentage Contribution to Lattice Energy	Dominating Interatomic Interaction Type	COOH % Contribution to Interaction	C ₆ H ₄ % Contribution to Interaction	NH ₂ % Contribution to Interaction
Aα1	1	8.2	-5.7	23.1	H-Bond	96.4	4.0	-0.4
Ca1	2	3.9	-5.4	21.8	π-π Stacking	14.5	72.6	13.0
Da1	1	7.9	-2.3	9.3	H-Bond	41.7	20.7	37.6
Ea1	1	7.8	-2.0	8.2	H-Bond	38.8	26.1	35.1
Fa1	2	8.0	-2.3	9.2	vdW	79.90	21.01	-0.92
Total			18.7	71.6				

3

b

Bond	Multiplicity	Distance (Å)	Intermolecular Energy (kcal/mol)	Percentage Contribution to Lattice Energy	Dominating Interatomic Interaction Type	COOH % Contribution to Interaction	C ₆ H ₄ % Contribution to Interaction	NH ₂ % Contribution to Interaction
Ba2	1	8.3	-5.6	22.9	H-Bond	96.7	3.6	-0.4
Ca2	2	3.9	-5.3	21.7	π-π Stacking	14.5	72.6	13.0
Da2	1	7.9	-2.3	9.3	H-Bond	41.7	20.7	37.6
Ea2	1	7.8	-1.2	4.9	H-Bond	38.8	26.1	35.1

F α 2	2	6.9	-1.9	7.7	vdW	80.8	20.0	-0.9
Total			-16.3	66.5				

1

2

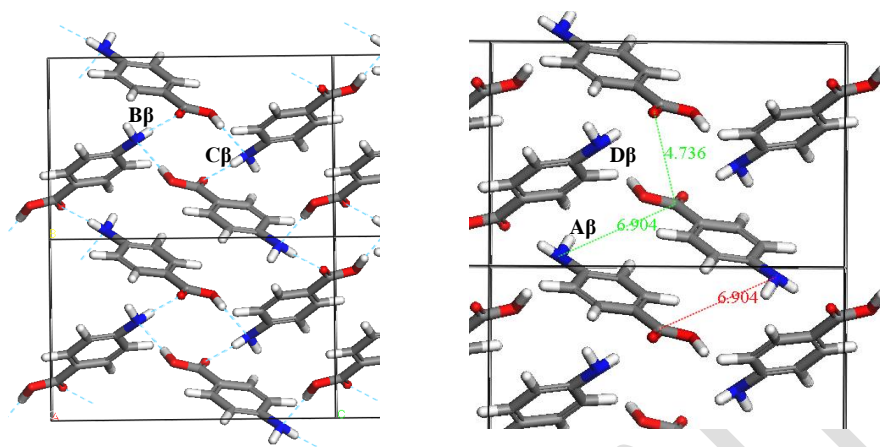
3

4

5

6

7

8 **Figure 6: Strongest interactions of β -*p*ABA labelled on the β packing diagram. Combination of**9 **H-bonding ring interactions (B and D) and offset stacking with interactions between the NH_2** 10 **and COOH groups (A and C) indicating that both types of interactions are important in the**11 **formation of β . Interactions tabulated in table 4**

12

13

14

15

16

17

18

19

20

1 **Table 4: Eight strongest intermolecular interactions from β -*p*ABA.**

Bond	Multiplicity	Distance (Å)	Intermolecular Energy (kcal/mol)	% Contribution to Lattice Energy	Dominating Interatomic Interaction Type	COOH % Contribution to Interaction	C ₆ H ₄ % Contribution to Interaction	NH ₂ % Contribution to Interaction
A β	1	4.17	-2.57	11.9	π - π stacking	33.3	65.2	1.5
B β	2	8.11	-2.45	22.7	H-Bond	46.5	15.7	37.7
C β	2	5.73	-2.39	22.2	vdW	37.8	34.0	28.2
D β	2	6.74	-1.46	13.6	vdW	9.1	44.5	46.4
E β	1	6.53	-1.01	4.4	vdW	15.7	80.21	4.1
Total			-16.18	74.8				

2

3 Figure 5 and table 3 shows that the strongest interactions in the α form were found to be the H-
4 bonding dimers between the carboxylic acid groups, contributing approximately 23% of the calculated
5 lattice energy. Interestingly bond C α , which involves the more isotropic vdW forces due to π - π
6 interactions between close packed molecules of *p*ABA stacking along the b-axis, was found to
7 contribute approximately 22% of the total calculated lattice energy. Figure 6 and table 4 shows the
8 contributions from the strongest interactions in the β -form is much more evenly spread in 3-
9 dimensions with respect to the α -form. The top four interactions all contribute above 10% of the
10 lattice energy. Of these, the two most important interactions (A β and C β) which each were found to

27

1 contribute around 22% to the lattice energy, are the OH...N H-bond and the polar interactions between
2 the two COOH head groups.

3 The functional group contribution analysis with respect to the lattice energy as highlighted in table 1
4 is further expanded in columns 7-9 in tables 3 and 4 by considering the difference in their %
5 contributions to the intermolecular interaction strengths, both within the ranked lists for each
6 polymorph, as well as between the polymorphic forms. For example, the carboxylic H-bonded dimers
7 ($A\alpha$) were found to have over 96% of its interaction centred on the COOH group, while the π - π
8 stacking interaction ($C\alpha$) was found to be more centred on the phenyl ring, with over 72% of the
9 interaction contributed by the phenyl ring.

10 These pair-wise synthonic interactions are shown in figure 7 and highlight the important bulk
11 synthons for each structure.

12

13

14

15

16

17

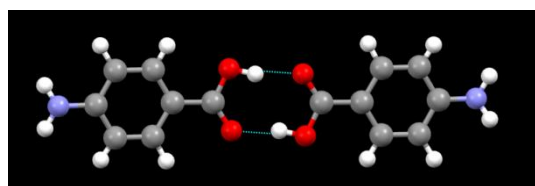
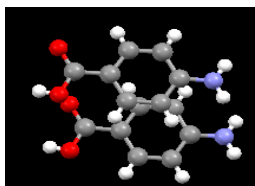
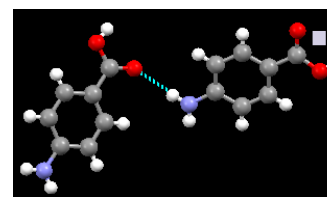
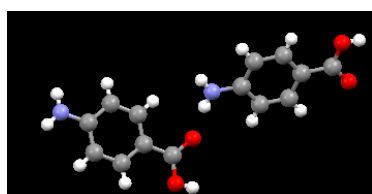
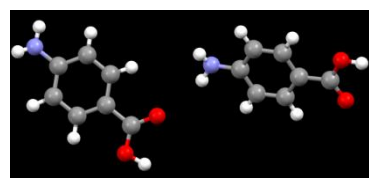
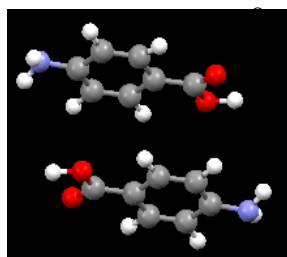
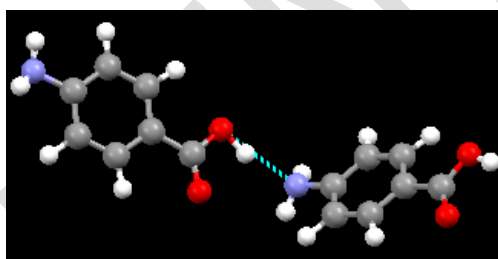
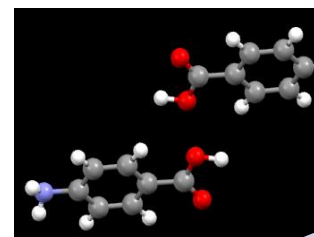
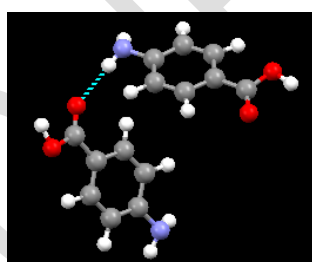
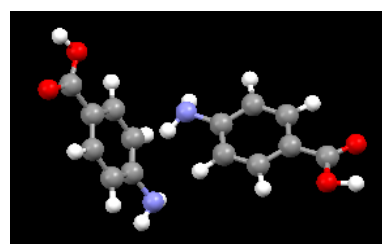
18

19

20

21

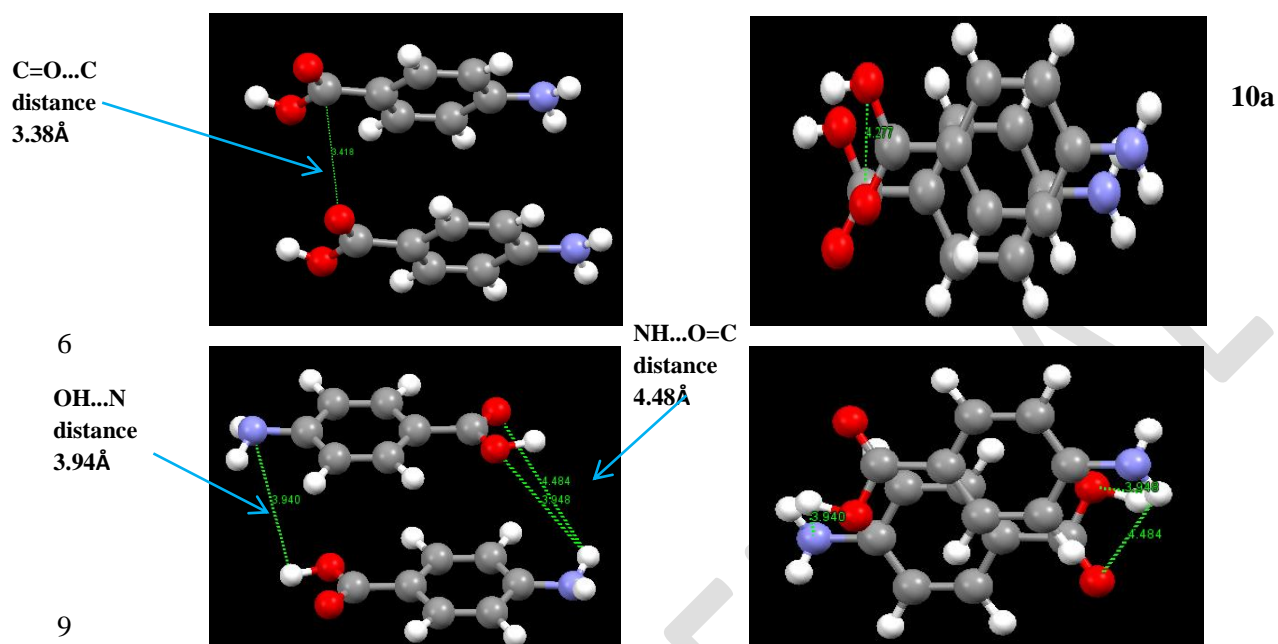
28

1 (a) α -*p*ABA Important Synthons4 **Aα1/Bα2**4 **Cα1/Cα2**4 **Dα1/Dα2**5 **Eα1/Eα2**6 **Fα2/Gα2**8 (b) β -*p*ABA Important Synthons12 **Aβ**12 **Bβ**12 **Cβ**13 **Dβ**13 **Eβ**

16 **Figure 7: Important bulk synthons as specified in tables 3 and 4 for both forms of *p*ABA that**
17 **are required to be satisfied to converge the lattice energy. Pairwise interactions visualised for**
18 **clarity. Combination of H-bonding and vdW interacting synthons important for both**
19 **structures.**

20

- 1 It is interesting to observe that both structures were found to contain a π - π stacking motif, with the α
 2 structure containing a head to head stack and the β structure containing a head to tail stack.



11 **Figure 8a:** (above left and right) α π - π stacking dimer, head to head stacking 3.8Å
 12 intermolecular distance between the corresponding NH₂ and COOH groups. Molecules slightly
 13 offset creating stronger interactions between the functional groups. **Figure 8b:** (below left and
 14 right) β π - π stacking. Head to tail stack around 4Å distance between functional groups.
 15 Molecules more offset than α to maximise strength of interactions between NH₂ and COOH
 16 groups.

17 Figure 8a shows the head to head α stacking motif. The stacking motifs Ca1 and Ca2 associated with
 18 the two different molecules in the asymmetric unit are almost identical and form a strong
 19 intermolecular interaction. The stacking is slightly offset so that the negative nitrogen and positive
 20 hydrogen atoms can form stronger atom-atom electrostatic interactions at one end, whilst the negative
 21 oxygen and positive carbon can interact in the same way at the other end.

30

1 Figure 8b shows the β motif to be a head to tail stacking dimer that is even more offset than that in the
2 α stacking motif. This suggests that the electrostatic interactions between the more polar atoms in the
3 NH_2 and COOH functional groups are the dominating atom-atom interactions in this dimer motif.
4 This is despite the interatomic distances of the strongly interacting atoms being slightly longer in the β
5 stack compared to that present in the α stack. This particular stacking motif was predicted to be the
6 strongest synthon in the β structure, although the energies of this interaction and the $\text{OH}\dots\text{N}$ and
7 $\text{NH}\dots\text{O}$ H-bonding interactions are very similar.

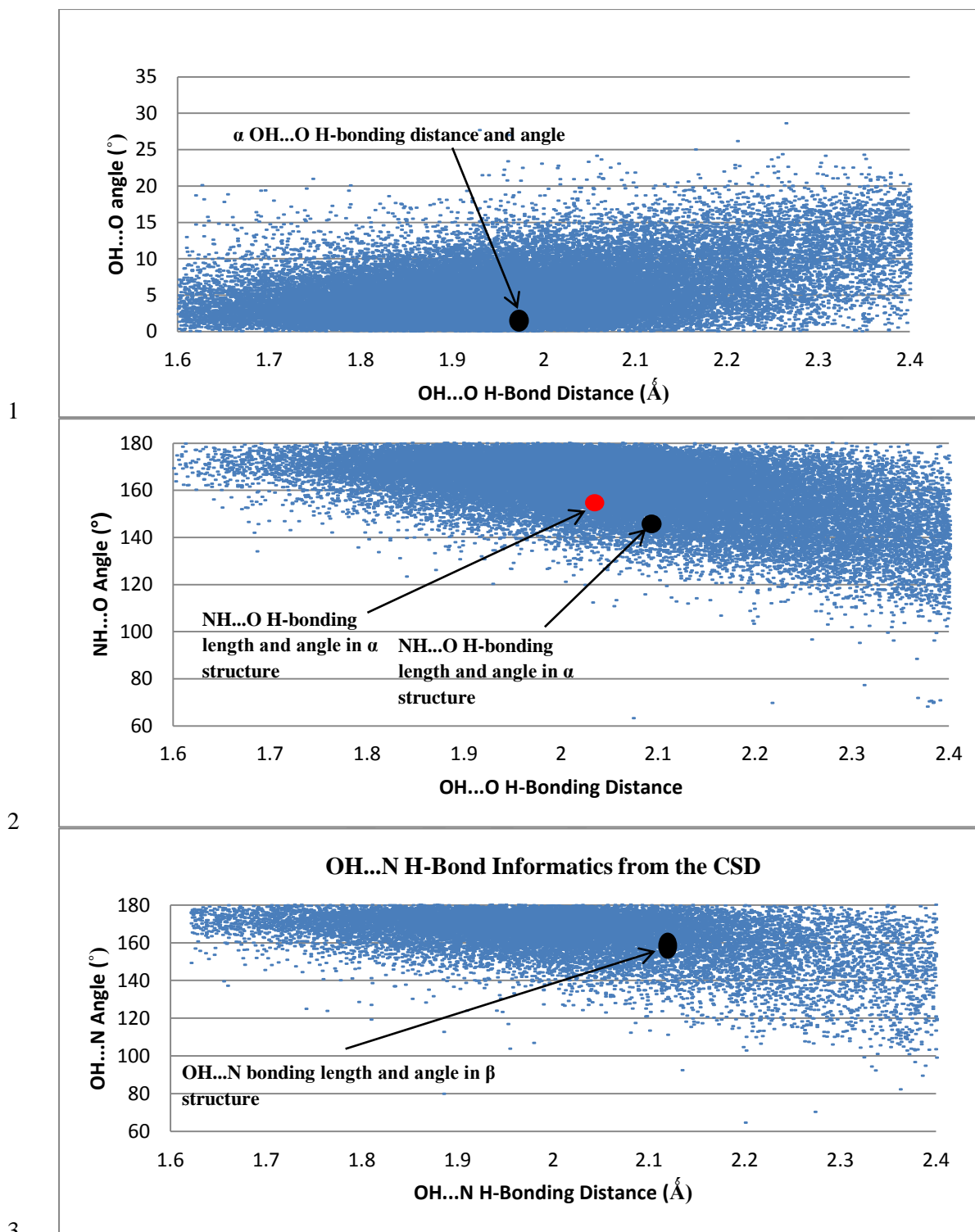
8 **4.4: CSD Analysis of Important H-Bonding Interactions**

9 Figure 9 shows the density of hits in the CSD of the $\text{OH}\dots\text{O}$, $\text{OH}\dots\text{N}$ and $\text{NH}\dots\text{O}$ interactions as
10 examined as a function of distance and angle:

11

12

CONFIDENTIAL



4 **Figure 9:** H-bonding data from the CSD of H-bonding angles and distances of OH...O (top),
 5 NH...O (middle) and OH...N (bottom) interacting groups. All interactions from the *p*ABA
 6 crystal structures were found to be in a dense area of hits suggesting these are stable common
 7 interactions.

32

1 Figure 9 revealed that the hit density of structures with OH...O H-bond lengths between 1.8Å and
2 2.1Å was very high. It also showed that the more linear the bond angle between the molecules, then
3 the higher the amount of hits. The H-bond length and orientation of the carboxylic acid H-bonding
4 dimer interactions in the α structure were found to be close to the centre of this dense area of
5 structures, consistent with this being a common and stable interaction.

6 The majority of the OH...N H-bonding interactions found in the search of the CSD were between
7 160° and 180° and had bond lengths of 1.8Å-2.1Å. The OH...N H-bonding length of 2.15Å in the β
8 structure was also found to be within a dense area of structures containing a similar bond length, once
9 again suggesting that this is a common stable interaction that is a key synthon in the molecular self-
10 assembly and formation of the β structure.

11 The spread of hits for the NH...O interactions in the CSD was found to be a little wider in terms of
12 bond length compared to the OH...O and OH...N interactions, though the highest density of hits was
13 found to be around 2Å. The shorter interactions tended to have more linear interactions, but as the
14 NH...O bond length increased, the bond angle was found to move away from a linear conformation,
15 suggesting that these structures could be more amenable to a change in geometry as the NH...O bond
16 length increases, mindful that these interactions would be expected to be weaker and possibly not the
17 major interactions that stabilise the crystal structure. This appears to be the case for the NH...O
18 interactions present in the α and β forms of *p*AABA.

19 **4.5 Morphological Simulations and Surface Chemistry Analysis**

20 **4.5.1: Attachment Energy Morphology Analysis**

21 The calculated attachment energies for the major faces as predicted by the BFDH model for both
22 forms are shown in table 5:

23

24

- 1 **Table 5a: Slice, attachment and anisotropy factor of the important faces predicted by the BFDH**
 2 **rule of α -pABA in monomer mode. Table 5b: Slice, attachment and anisotropy factor of the**
 3 **important faces predicted by the BFDH rule of α -pABA in dimer mode. Table 5c: Slice,**
 4 **attachment and anisotropy factor of the important faces predicted by the BFDH rule of β -pABA.**

Face (hkl)	d_{hkl} (Å)	Slice Energy (kcal/mol)	Attachment Energy (kcal/mol)	% Saturation of Surface Molecule (Anisotropy Factor)
1 0 1	12.7	-24.5	-1.7	93.6
1 0 -1	13.6	-14.1	-10.4	66.2
0 1 -1	3.8	-9.2	-15.4	35.9
1 1 -1	3.7	-8.2	-16.3	34.6
1 -1 0	3.8	-9.1	-15.5	39.5
0 0 2	9.3	-14.7	-9.6	59.8
2 0 0	9.3	-15.0	-9.8	60.5

5

Face (hkl)	d_{hkl} (Å)	d_{hkl} (Å)	Slice Energy (kcal/mol)	Attachment Energy (kcal/mol)	% Saturation of Surface Molecule (Anisotropy Factor)
1 0 1	12.7	5.2	-26.6	-8.3	76.1
1 0 -1	13.6	6.0	-20.7	-14.3	59.2
0 1 -1	3.8	7.0	-9.4	-25.4	27.0

34

1 1 -1	3.7	4.9	-7.6	-27.3	21.8
1 -1 0	3.8	5.0	-8.5	-26.4	24.4
0 0 2	9.3	6.1	-20.7	-14.2	59.3
2 0 0	9.3	3.1	-21.5	-13.4	61.6

1

Face (hkl)	d_{hkl} (Å)	Slice Energy (kcal/mol)	Attachment Energy (kcal/mol)	% Saturation of Surface Molecule (Anisotropy Factor)
0 1 1	5.2	-12.2	-10.5	53.8
0 0 2	6.0	-8.9	-13.8	39.2
1 0 -1	7.0	-10.6	-12.2	46.5
1 0 1	4.9	-12.0	-10.7	53.0
1 1 1	5.0	-10.5	-12.2	46.2
1 1 0	6.1	-11.5	-11.2	50.8
1 1 -1	3.09	-8.34	-14.39	36.69

2

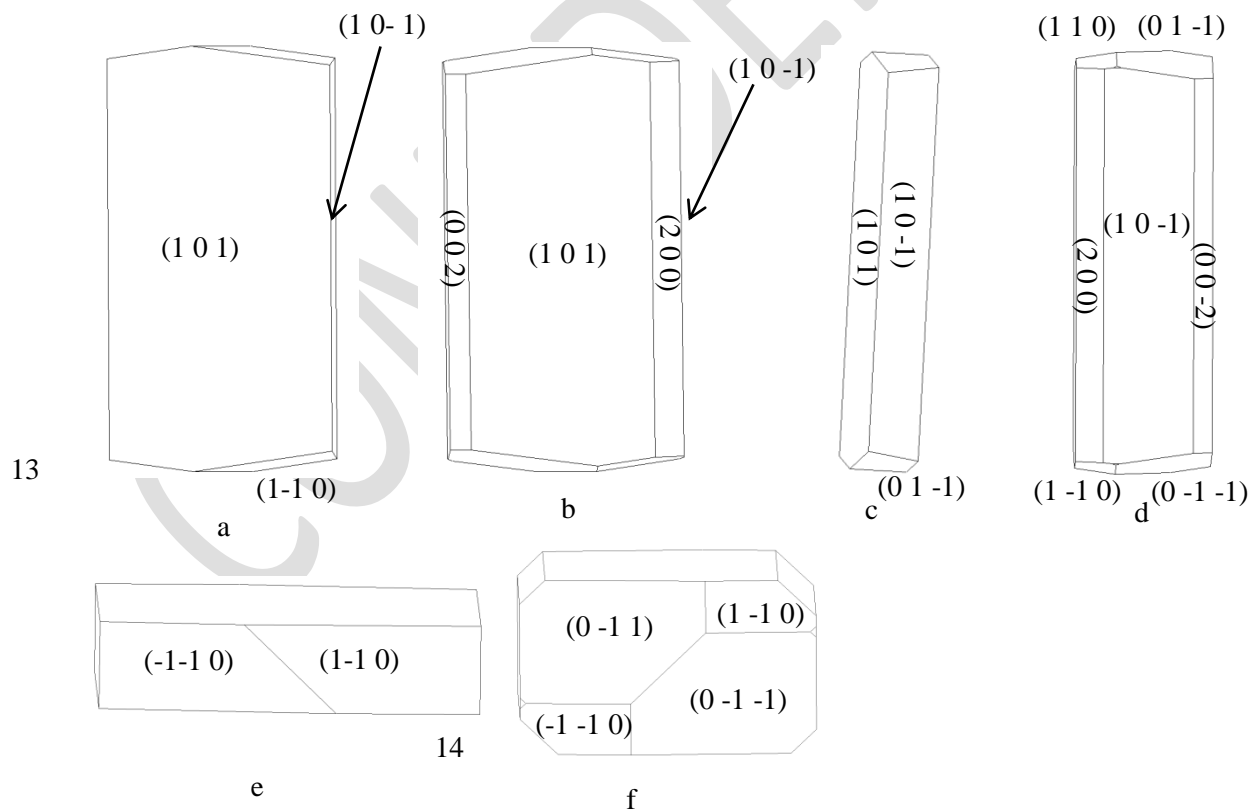
3 The degree of satisfaction of the intermolecular interactions of a molecule at a surface compared to a
 4 molecule in the bulk can be related to how labile a surface is to accepting molecules from solution and
 5 therefore how fast a given surface will grow. Table 5a shows the degree of satisfaction of a molecule
 6 within the α -structure for the different faces from the monomer binding calculation is markedly
 7 diverse, with the slow growing (1 0 1) surface having approximately 93% of possible interactions

1 satisfied. Compared to the capping (0 1 -1), (1 -1 0) and (1 1 -1) surfaces, which have approximately
 2 35-39% of interactions satisfied. Hence, it can be expected that the capping faces would grow
 3 significantly faster than the (1 0 1) surface.

4 4.5.2 Confrontation of Morphological Simulation to Experimental Data

5 4.5.2.1 α -form

6 The attachment energies for the monomeric growth unit model in table 5a resulted in the flat lath-
 7 like morphological prediction shown in figure 10a and c. A comparison of the attachment energies
 8 calculated for α -pABA using the dimer growth unit, revealed that the attachment energy of the (1 0 1)
 9 surface is increased when compared to that calculated for the monomer form, with the attachment
 10 energies of the (1 0 -1) and the capping surfaces being relatively reduced. This reduction of the
 11 attachment energy of the capping surfaces resulted in the prediction of a less plate like morphology
 12 shown in figure 10b and d, with the predicted inclusion of the (0 0 2) and (2 0 0) surfaces.



15 **Figure 10a, c and e: Attachment energy morphological prediction of α -pABA, assuming the**
 16 **attaching growth units are monomers, showing the major faces that are predicted in the final**
 17 **morphology. Figure 10 b, d and f: Attachment energy morphological prediction of α -pABA,**

36

1 assuming the attaching growth units are carboxylic acid H-bonding dimers, showing the major
2 faces that are predicted in the final morphology.

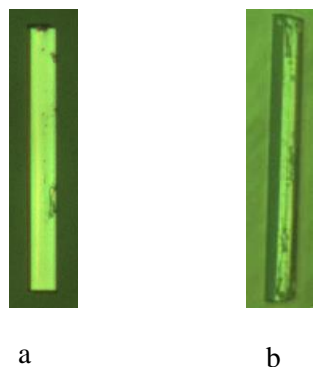
3

4

5

6

7

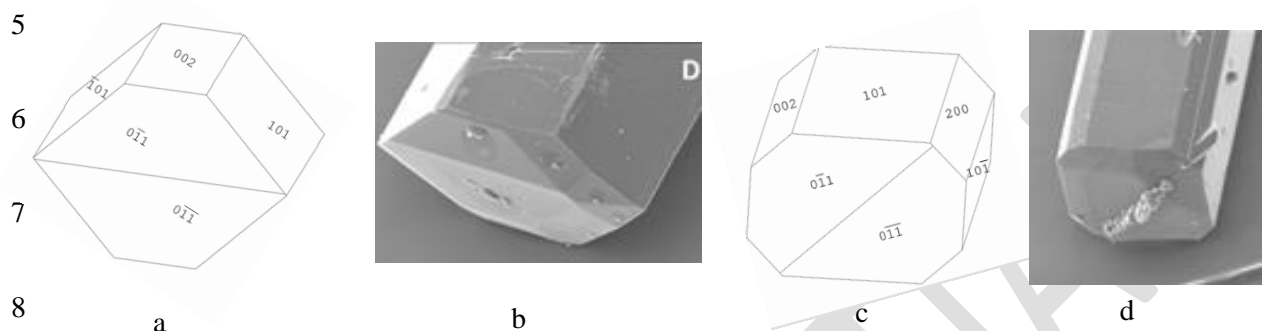


8 **Figure 11a: α -pABA grown in EtOH at $\sigma = 0.03$ for ten mins. Figure 11b: α -pABA grown in**
9 **EtOH at $\sigma = 0.07$ for ten mins.**

10 Both monomer and dimer based morphological simulations have lower aspect ratios with respect to
11 those observed from the experimentally grown crystals shown in figure 11. Studies of the crystal
12 growth rates for the capping faces of α -pABA is consistent with their growth by a linear dependence
13 of the growth rate as a function of supersaturation, suggesting a rough interfacial growth mechanism
14 (RIG). This reflects the strong intermolecular solute/surface recognition from the solution phase to
15 crystal habit surface due to the strong π - π stacking interactions⁵⁶. In contrast, the side (1 0 -1) surfaces
16 were found to grow by a B&S mechanism⁵⁶. The attachment energy morphology is essentially a
17 prediction of the growth morphology under equilibrium conditions, i.e. at zero supersaturation, and
18 this provides a good prediction for crystals that grow by a BCF¹⁴ or B & S¹⁵ mechanism. This higher
19 growth rate for the capping face, with respect to that of the side faces, probably explains why the
20 growth (kinetic) morphology is less consistent with the predicted equilibrium morphology.

21 Figure 11a shows that at very low supersaturations α -pABA appears to present a more flat and lath-
22 like morphology. Though still longer than the monomer morphology prediction, the general flat shape
23 appears to correlate to the low supersaturation crystal featuring a dominant flat face being the (1 0 1)
24 surface. Figure 11b shows at $\sigma = 0.07$, the shape of the crystal appears thicker and seems to include

1 more faces in the b-axis zone of the crystal, probably the (0 0 2) and (2 0 0) surfaces that appear in the
 2 dimer morphological prediction. Recent work by Sullivan and Davey suggests that the (1 0 1) and (1 0
 3 -1) surfaces do not completely dominate the b-axis zone of facets (figure 12 b and d), and that the
 4 morphology is 6 or even 8 sided, with increased importance of the (0 0 2) face⁶⁴.



9 **Fig 12a: 6-sided morphological sketch of α -pABA adapted to match figure 12b. Figure 12b: α -**
 10 **pABA crystal grown from slow solvent evaporation of EtOH. Figure 12c: 8-sided morphological**
 11 **sketch adapted to match figure 12d. Figure 12d: α -pABA crystal grown from slow solvent**
 12 **evaporation of EtOAc. Figure 12b and d reproduced with permission from Sullivan and Davey**
 13 **CrystEngComm, 2014⁴⁹.**

14 The morphological sketch in figure 12a suggests that in the 6 sided shape in figure 12b, the extra face
 15 is indeed the (0 0 2) surface. However, the morphological sketch in figure 12c suggests that both the
 16 (0 0 2) and (2 0 0) faces can be present in the growth morphology of α -pABA. Table 5a and b show
 17 that the predicted attachment energy for these minor habit surfaces were found to be very similar to
 18 each other for both the monomer- and dimer-based calculation. The latter would suggest that the
 19 growth rates for these faces would be very similar and, hence, there would be a competition between
 20 these two faces in terms of them appearing in the final growth morphology. Table 6 shows
 21 experimental interplanar angles in the (0 1 0) zone for an α -pABA crystal with respect to those
 22 calculated based on the unit cell parameters.

1 **Table 6: Consecutive measurement of interplanar angles of an α -*p*ABA crystal grown from slow**
 2 **solvent evaporation of ethanol matched with the faces via calculated angles.**

Plane angle measured	Calculated angle (°)	Measured Angle (°)
(0 0 2) → (1 0 1)	43.3	43
(1 0 1) → (2 0 0)	43.13	45
(2 0 0) → (1 0 -1)	46.69	46

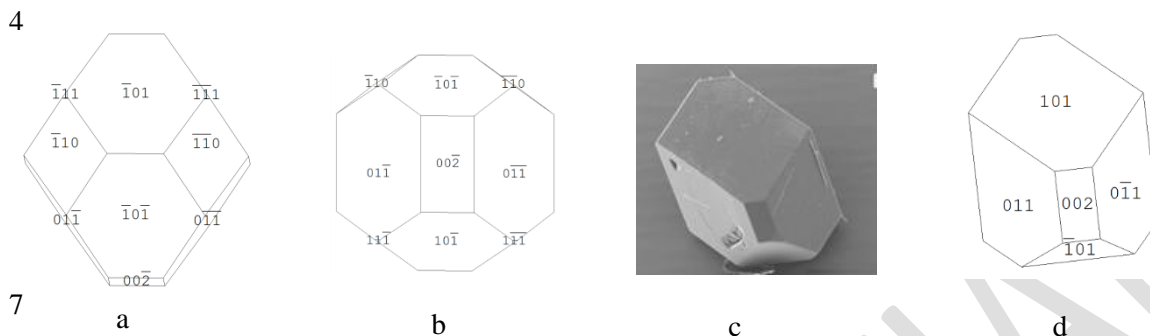
3 The interplanar angles were found to match reasonably well to the calculated interplanar angles,
 4 suggesting the appearance of the (0 0 2) and (2 0 0) faces in the experimental crystal morphology that
 5 are shown in figure 12c.

6 As with the b-axis zone of the crystal facets, the end capping faces also appeared to show variations in
 7 the final experimental growth morphology with respect to predictions. The monomer attachment
 8 energy prediction (figure 10e) showed the (1 -1 0) and (-1 -1 0) faces at the end of the crystal.
 9 However, comparison of calculated and measured interplanar angles between the edge (1 0 -1)
 10 surfaces and with those of the capping faces suggested that the capping face is more likely to be the (0
 11 1 -1) face. That said, the attachment energies of the (0 1 -1) and (1 -1 0) faces were seen to be very
 12 similar (table 5a), suggesting that the appearance of these faces at the capping end of the crystal is
 13 very competitive.

14 **4.5.2.2 β -form**

15 The attachment energy, and hence the anisotropy factor, for the morphologically important surfaces of
 16 the β -form were found to be relatively similar, and thus, more isotropic growth would be expected in
 17 3D. Figure 12a and b show the attachment energy morphological prediction of β -*p*ABA to have a
 18 diamond-shaped morphology, with more equal growth in the different crystallographic directions.
 19 This is consistent with the attachment energies calculations given in table 5c.

1 The attachment energy prediction for the β polymorph compared to experimentally grown crystals is
 2 shown in figure 13a and b and shows that the morphological prediction this gives a good match to the
 3 shape of the experimentally grown β -*p*ABA crystal shown in figure 13c.



8 **Figure 13a and b: Attachment energy morphological predictions of the crystal structure of β -**
 9 ***p*ABA. Figure 13c: SEM of β -*p*ABA grown from water showing flat top face, no evidence of**
 10 **multi faceting. Figure 13d: Morphological sketch of β -*p*ABA made to resemble the experimental**
 11 **crystal in figure 13c. Figure 13c reproduced with permission of Sullivan and Davey,**
 12 **CrystEngComm, 2015⁴⁹.**

13 However, the simulation shown in figure 13a shows a multifaceted top surface, whereas figure 13c
 14 shows a flat top surface. From the morphological sketch in figure 13d, it would appear likely that the
 15 dominating top face is the (1 0 1) surface. Table 5c shows that the attachment energies of the
 16 individual faces of β -*p*ABA were found to be similar, suggesting that the growth rates are quite
 17 similar to each other and hence the associated crystal growth mechanisms are probably the same. This
 18 is in contrast to α -*p*ABA and is probably a factor as to why the attachment energy morphological
 19 prediction of β -*p*ABA gave a greater resemblance to experimental crystals when compared to α -
 20 *p*ABA.

21

22

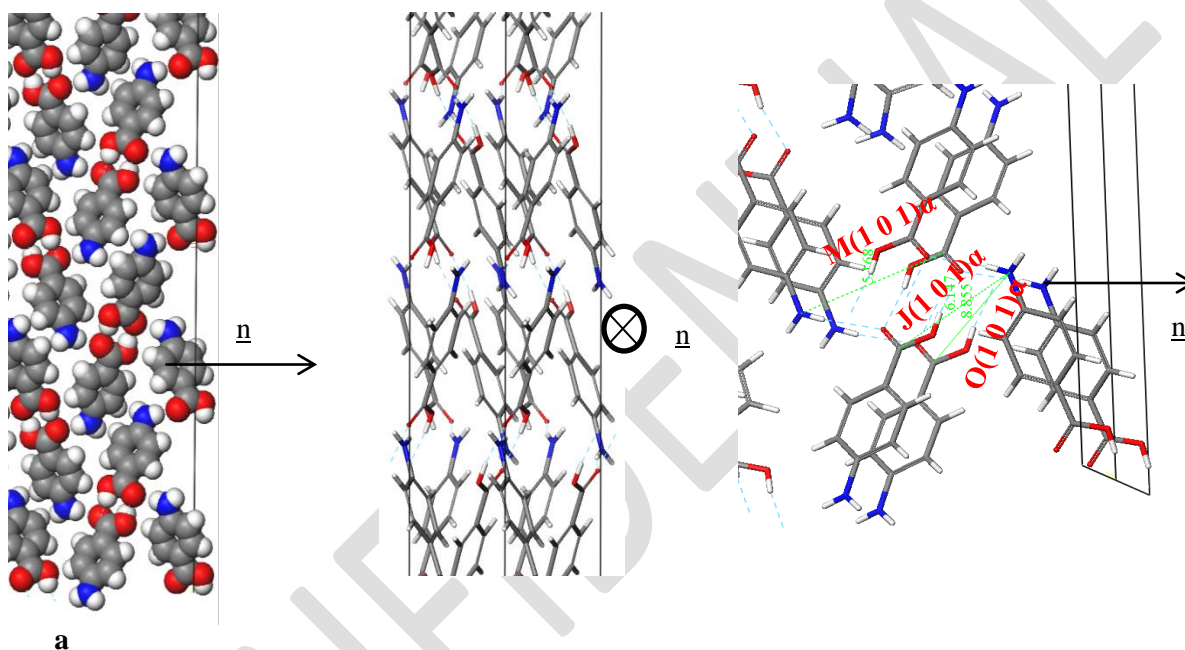
23

24

40

1 **4.5.3: Surface Chemistry Analysis**2 **4.5.3.1 α -Form**

3 The previous analysis of the intermolecular interactions was from the bulk crystal structure (figure 6,
 4 table 4). In this case, the specific unsaturated interactions that contribute to the attachment energy at
 5 each of the present surfaces were characterised for the monomer attachment energy prediction of both
 6 forms.



7 **a**
 8 **Figure 14: Crystal chemistry of the (1 0 1) surface of α -pABA: (a) space fill model of side view;**
 9 **(b) stick model of plan view; (c) stick model of side view.**

10 **Table 7: Extrinsic synthons contributing to the attachment energy of the α -pABA (1 0 1)**
 11 **surface. Strongest interaction contributing to (1 0 1) growth is the Jth strongest in the bulk**
 12 **interactions, hence slow growth.**

Bond	Multiplicity	Distance (Å)	Intermolecular Energy (kcal/mol)
J(1 0 1) α	2	6.9	-0.7
M(1 0 1) α	2	6.7	-0.4

O(1 0 1) α	2	8.9	-0.2
-------------------	---	-----	------

1 Figure 14a shows that the carboxylic acid H-bonding dimers were found to run in-plane at the (1 0 1)
2 surface. Figure 14b shows the π - π stacking in the b direction was found to be perpendicular to the
3 growth direction of the (1 0 1) surface, and therefore not contributing to the attachment energy. Table
4 7 shows the extrinsic synthons were found to be made up of vdW interactions between the polar
5 atoms of the COOH and NH₂ functional groups. These interactions were found to be quite weak with
6 all of them being less than 1kcal/mol, hence the very low attachment energy predicted at this surface.
7 Compared to the strongest bulk interactions, e.g A, B and C representing the H-bonding carboxylic
8 acid dimers and π - π stacking interactions, the strongest interaction for this face was found to be
9 comparatively weak and is 10th (Jth) in terms of morphological importance. Such a low attachment
10 energy and concomitantly weak interactions at this surface would be consistent with a slow growth
11 rate for this surface.

12

13

14

15

16

17

18

19

20

21

22

42

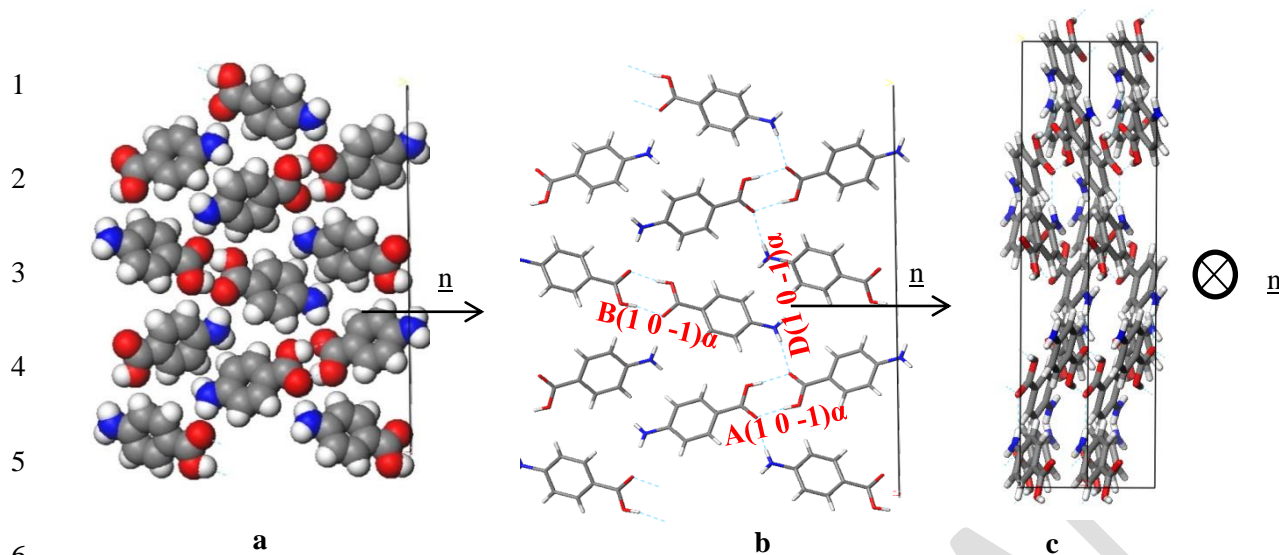


Figure 15: Crystal chemistry (1 0 -1) surface of α -pABA: (a) space fill model of side view; (b) stick model of side view; (c) stick model of plan view

Table 8: Extrinsic synthons contributing to the attachment energy of the α -pABA (1 0 -1). Strongest interactions contributing to the attachment energy are the 1st, 2nd and 4th strongest from the bulk interactions.

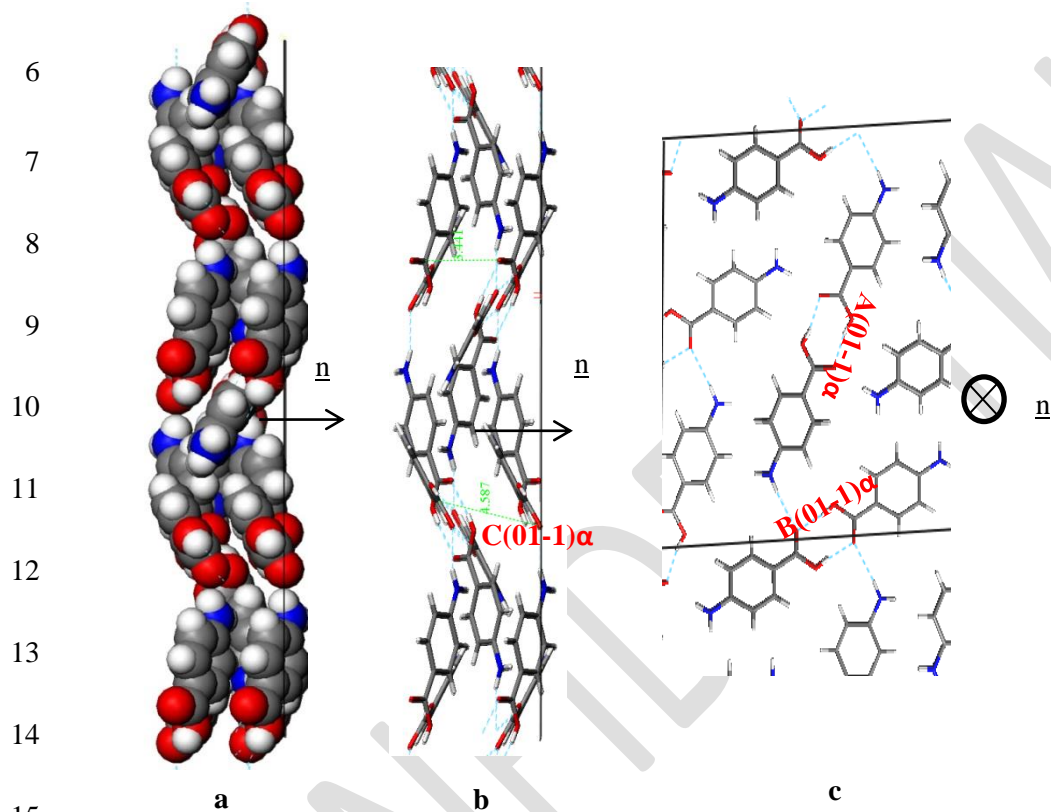
Bond	Multiplicity	Distance (Å)	Intermolecular Energy (kcal/mol)
A(10-1) α	1	8.2	-5.7
B(10-1) α	1	8.3	-5.6
D(10-1) α	2	7.9	-2.3

Figures 12a and 12b shows the COOH and NH₂ functional groups were found to be orientated almost parallel to the direction of growth of the α -pABA (1 0 -1) surface. The H-bonds between the COOH groups were found to form almost parallel to the growth direction of this surface, hence promoting much faster growth in this direction when compared to that of the (1 0 1) surface. Figure 12c shows reactive H-bonding functional groups exposed at this surface, while the π - π stacking were found to form almost perpendicular to this surface and are therefore would not be involved with the growth of

43

1 the (1 0 -1) surface. Table 7 shows that the interactions contributing to the attachment energy for this
2 surface were found to be some of the strongest bulk interactions with the attachment energy predicted
3 to be more than five times higher than that for the (1 0 1) surface.

4 The capping face (0 1 -1) was predicted to be the fastest growing of the morphologically important
5 crystal surfaces.



16 **Figure 16: Crystal chemistry of (0 1 -1) surface of α -pABA: (a) space fill model of side view; (b)**
17 **stick model of side view; (c) stick model of plan view**

18

19

20

21

22

1 **Table 9: Extrinsic synthons contributing to the attachment energy of the (0 1 -1) surface.**

2 **Strongest interactions at (0 1 -1) are the 3 strongest from the bulk interactions.**

Bond	Multiplicity	Distance (Å)	Intermolecular Energy (kcal/mol)
A(01-1) α	1	8.2	-5.7
B(01-1) α	1	8.3	-5.67
C(01-1) α	2	3.9	-2.7

3 Figure 16a of the space fill model shows how the molecules were found to close pack in zig-zag
 4 chains stacking along the b direction of the structure. The molecules were found pack more closely
 5 along this growth direction than the (1 0 1) or (1 0 -1) directions, and hence it is no coincidence that
 6 the (0 1 -1) surface was found to grow much faster than the (1 0 1) or (1 0 -1) habit surfaces. Figure
 7 16b shows the C intermolecular interaction that represent the intermolecular interactions created by
 8 the close π - π packing, and this interaction was found to be close to parallel with respect to the
 9 direction of growth. Table 9 shows the three strongest interactions contributing to the attachment
 10 energy at this surface, which were found to be the same as the three strongest interactions measured
 11 for the bulk interactions.

12 The attachment energy model also predicted contribution from the OH...O intermolecular interactions
 13 between the H-bonding dimers to the growth of this surface. However, examining the in-plane
 14 molecular packing of the (0 1 -1) surface revealed that these interactions are not orientated
 15 significantly along the growth direction of this surface, which would be consistent with their reduced
 16 role in the growth of the (0 1 -1) surface.

17 These orientation effects then suggest that the dominant interactions promoting the fast growth of the
 18 (0 1 -1) surface are the π - π stacking interactions. The close packing is very favourable and coupled
 19 with the fact that the solvents used for crystallisation have strongly contrasting molecular structures,
 20 i.e. without any aromatics, would suggest that the surface/solvent interaction would be unlikely to
 21 disrupt this interaction and hence the growth process of the (0 1 -1) surface.

45

1 In this respect, it is also important to consider that α -*p*ABA crystallises from polar protic solvents
2 such as EtOH, MeOH etc. which can form strong H-bonds and thus each growing surface must de-
3 solvate before incorporation of solute and growth can occur. The (1 0 -1) surface was found to have
4 exposed H-bonding sites orientated directly out at the surface, not only having potential to form
5 strong interactions with *p*ABA, but also with H-bonding solvents. Such binding would have the effect
6 of slowing down the de-solvation process, and hence through this the growth rate of the surface. In
7 comparison to the capping (0 1 -1) surface, where the growth process was found to be dominated by
8 the π - π solute binding interactions, the solvent binding strength for polar protic solvents would be
9 expected to be much lower and hence the solvent effect on the growth process would be expected to
10 be relatively low. Such a solvent binding effect on the (1 0 -1) surface might be a further factor
11 explaining the discrepancy between the predicted and observed morphology i.e. reflecting the fact that
12 the actual solvent-mediated growth rate could be much lower than that predicted.

13 4.5.3.2: β -form

14 Figure 13 reveals the (0 1 -1) face is the largest face visible at the surface, but it does not dominate to
15 the same extent as the (1 0 1) face in the α form. The (1 1 0), (1 0 1) and (1 0 -1) faces also contribute
16 significantly to the surface area of the crystal habit. The analysis of the unsaturated synthons at the β
17 faces present at the crystal surface was performed with the approach used for the α form.

18

19

20

21

22

23

24

46

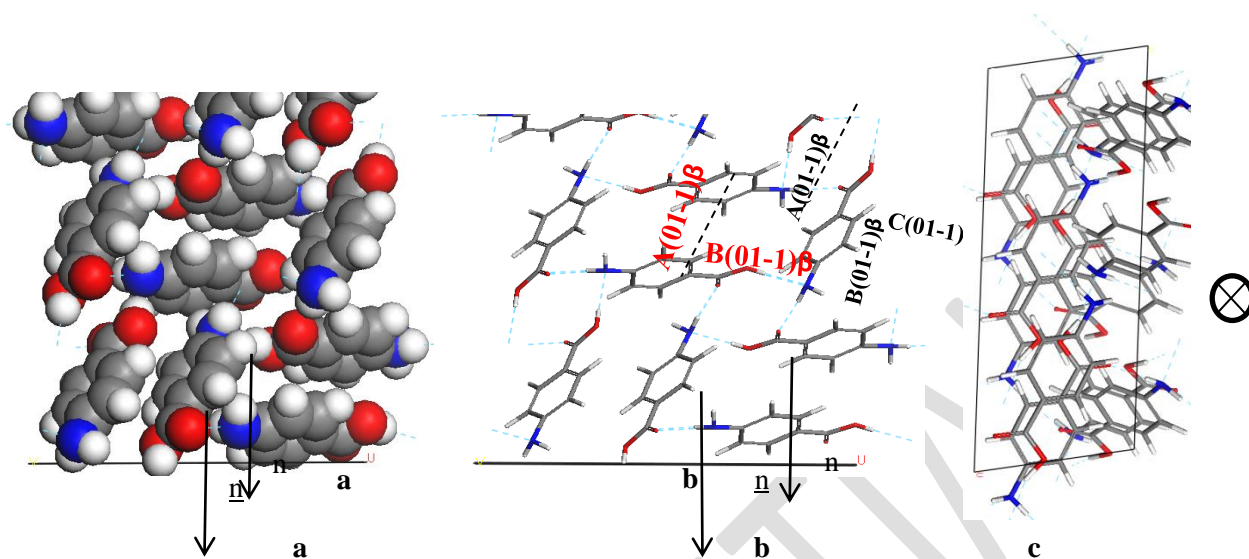


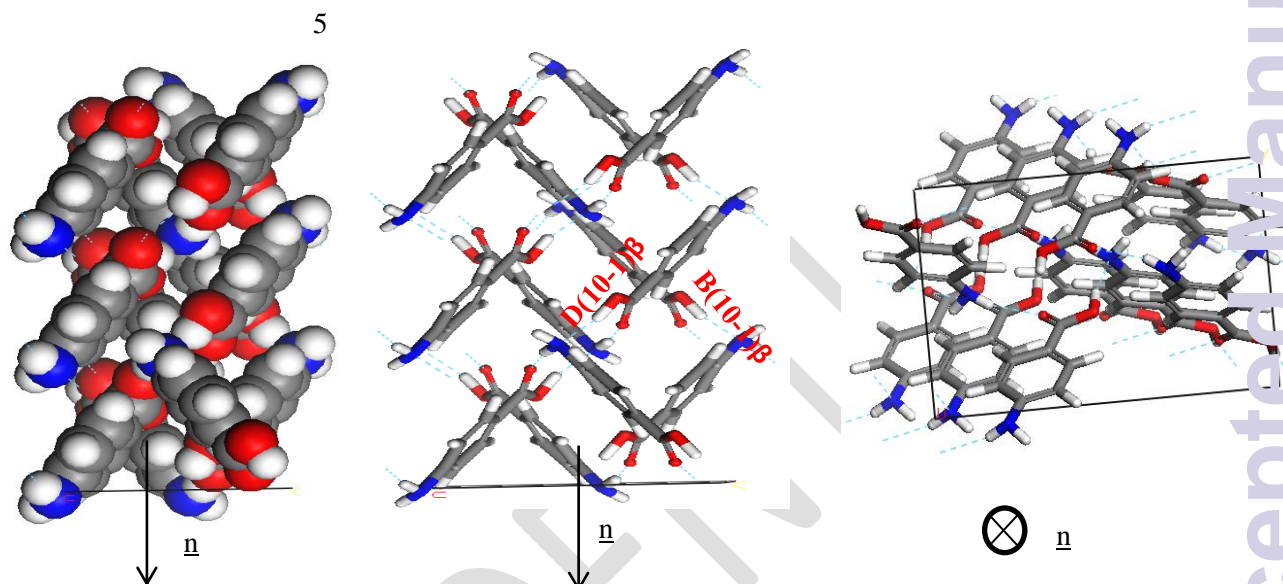
Figure 17: Crystal chemistry of (0 1 -1) surface of β -pABA: (a) space fill model of side view; (b) stick model of side view; (c) stick model of plan view

Table 10: Extrinsic synthons contributing to the attachment energy of the β -pABA (0 1 -1) surface. Top 3 interactions contributing to the attachment energy same as the 3 strongest interactions from the bulk interactions.

Bond	Multiplicity	Distance (Å)	Intermolecular Energy (kcal/mol)
A(0 1 -1) β	1	4.2	-2.6
B(0 1 -1) β	2	8.1	-2.5
C(0 1 -1) β	1	5.7	-2.4

Analysis of the (0 1 -1) surface revealed that it has exposed NH_2 and COOH groups that form the 4-membered H-bonding ring. The molecules were also found to stack out of the plane of this face to form the head to tail π - π stacking, hence table 10 shows that the strongest interactions contributing to the attachment energy of this face were found to be in fact the same as the strongest bulk interactions.

1 Figure 14a of the space fill model shows how the molecules stack almost perpendicular to each other,
 2 resulting in more equal growth in different directions, consistent with the isotropic nature of the
 3 morphology observed for the β -form. The same can be observed for the NH...O and OH...N H-
 4 bonding interactions.



13 **Figure 18: Crystal chemistry of (1 0 -1) surface of β -pABA: (a) space fill model of side view; (b)**
 14 **stick model of side view; (c) stick model of plan view**

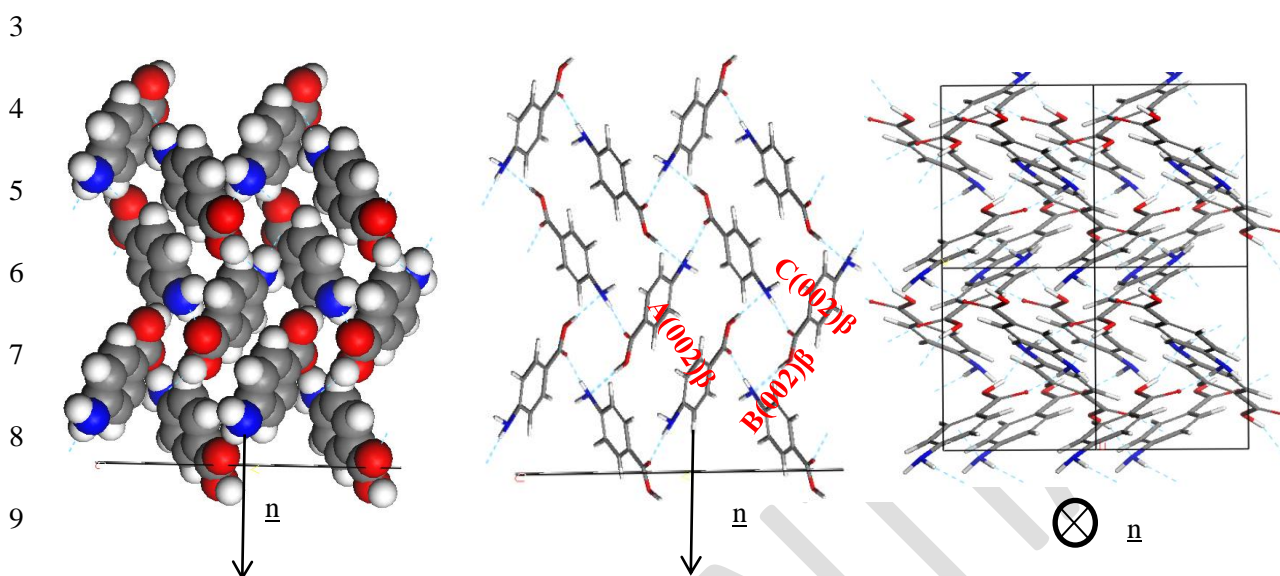
15 **Table 11: Extrinsic synthons contributing to the attachment energy of the pABA β (1 0 -1)**
 16 **surface. B and D H-bonding interactions contributing as stacking interactions are orientated**
 17 **away from the direction of growth.**

Bond	Multiplicity	Distance (\AA)	Intermolecular Energy (kcal/mol)
B(1 0 -1) β	2	8.1	-2.5
D(1 0 -1) β	2	6.7	-1.5

18 The pABA molecules were found to stack close to perpendicular to the β -(1 0 -1) surface growth
 19 direction and hence the stacking interactions were found not to contribute to the attachment energy of
 20 this surface. The OH group and the nitrogen were found to be orientated almost parallel to the growth

48

1 direction of the (1 0 -1) surface, and hence these interactions were found to dominate the growth of
 2 this surface



10 **Figure 19: Crystal chemistry of (1 0 -1) surface of α -pABA: (a) space fill model of side view; (b)**
 11 **stick model of side view; (c) stick model of plan view**

12 **Table 12: Extrinsic synthons contributing to the attachment energy of the β -pABA (0 0 2)**
 13 **surface. 3 strongest interactions contributing to attachment energy are same as 3 strongest**
 14 **interactions from bulk structure, reflecting faster growth of this surface.**

Bond	Multiplicity	Distance (Å)	Intermolecular Energy (kcal/mol)
A(002) β	1	4.2	-2.6
B(002) β	2	8.1	-2.5
C(002) β	1	5.7	-2.4

15

16 The smaller faster growing (0 0 2) surface was found to have contributions from the H-bonding and π -
 17 π stacking interactions to the growth of this face. The zig-zag chains of OH...N and NH...O hydrogen
 18 bonds making up the 4-membered ring structure were observed to run closer to the growth direction
 19 of the (0 0 2) surface compared to the other important surfaces present in the β morphology.

1 Figure 19c reveals that the phenyl rings are found to be at about a 45° tilt away from parallel to the
2 growth direction showing that there is some contribution to growth from the π - π stacking interactions
3 as well as the H-bonds formed to the exposed NH_2 group. Table 12 shows that all three of the
4 strongest bulk interactions were found to contribute to the attachment energy of this surface.

5 The strength and character of the extrinsic synthons associated with the major faces of the β form
6 were found to be not dissimilar to the synthons found at the surface of the smaller faster growing
7 faces. The more isotropic nature of the β packing which is dominated by the H-bonding ring means
8 that the major interactions were found to be orientated in more than one crystallographic direction;
9 hence they affect growth in different directions in 3D. The large, slow growing, (0 1 -1) and faster
10 growing (0 0 2) surface were also found to have significant contributions from all of the 4 strongest
11 intermolecular interactions. However, the amount of these interactions outside of the slice is found to
12 be less in the (0 1 -1) surface than the (0 0 2) surface, hence the larger predicted area of this face at the
13 surface. The (1 0 -1) surface has only two strong intermolecular interactions outside the slice, but
14 there was found to be a large contribution from both interactions, hence it has a smaller area than the
15 (0 1 -1) surface but a larger area than the (0 0 2).

16 4.5.4 Comparison between the α and β Morphologies

17 This isotropic nature of the distribution and strength of the synthons in 3 dimensions found within the
18 β structure is consistent with the attachment energy prediction more closely reproducing the
19 experimental crystal compared to the α form. The variation in nature and strength of the faces in the α
20 form suggest that the effect of solvent binding on growth rate will vary face to face, while the
21 interaction with solvent at the faces of the β crystal will be similar at each face, hence the
22 experimental solvent mediated morphology was found to be much the same as the morphology
23 predicted in the vacuum state.

24 Experimentally it appears that the growth via π - π stacking in the α form was found to be more
25 dominant than observed in the β form. Interestingly the amino hydrogens also showed a similar
26 contribution for both polymorphs. This could suggest the $\text{NH}\dots\text{O}$ interaction, that seems relatively

50

1 unimportant for the α form, could facilitate the transition pathway between the α and β form as it is
2 the main interaction that is found to be shared by both forms.

3 **5. Conclusions**

4 In this paper, the strength of the intermolecular interactions of *p*ABA were calculated and their
5 contribution to the lattice energy and morphology predictions of each polymorph was rigorously
6 analysed for the first time.

7 The NH_2 group of the β form was found to contribute more to the lattice energy than the NH_2 of the α
8 form, reflecting the H-bonding donor and acceptor role that the NH_2 plays in the β crystal structure,
9 compared to the NH_2 acting solely as a H-bonding donor in the α structure. The COOH group was
10 found to contribute significantly more to the lattice energy of the α form than the β form due to the
11 formation of the strong carboxylic acid H-bonding dimers. In addition, the formation of these H-
12 bonding dimers appears to hold the carboxylic acid groups rigidly planar with respect to the phenyl
13 ring in the α structure, while the β carboxylic acid group was found to have a slight torsion angle of
14 around 10° .

15 The morphological prediction of α -*p*ABA with a monomer growth unit gave a flat, lathe like
16 morphology, while prediction with a carboxylic acid dimer growth unit gave a less plate like
17 morphology. Both of these morphologies were predicted to have a large (1 0 1) surface, and it is
18 observed that the (1 0 1) surface interactions consist of weak vdW forces. Compared to the surface
19 interactions of the side (1 0 -1) which were found to contain H-bonding interactions, and the capping
20 faces which were found to contain π - π stacking interactions, these much weaker interactions result in
21 a much slower growth rate for the (1 0 1) surface. The experimental morphology often appears much
22 more needle like than the prediction. However, such morphological predictions reflect an equilibrium
23 situation, i.e. zero supersaturation, while the experimental morphologies are, by definition, grown
24 under supersaturated conditions. As seen from a previous study⁵⁶, the capping faces were found to
25 grow by a linear growth rate dependence with respect to supersaturation consistent with an RIG

1 mechanism. Hence, the equilibrium morphological predictions would not be expected to predict the
2 relative growth rates of a 3D set of surfaces crystallised under different interface kinetic mechanisms.

3 The dimer morphological prediction included the (2 0 0) and (0 0 2) surfaces, and comparison of
4 some of the images from the publication by Sullivan and Davey⁴⁹ to morphological sketches suggest
5 that these faces can indeed appear in the α morphology. This assertion was reinforced by interplanar
6 angle measurements from optical goniometry. However, optical microscopy at differing
7 supersaturation suggests that the morphology can vary in different conditions, and that it is not as
8 simple as one set morphology for the α form.

9 Comparatively, the β morphological prediction gave a reasonable match to the general shape of the
10 experimental crystal. There seemed to be an underestimation of the morphological importance of the
11 (1 0 1) surface. The higher resemblance of the β morphological prediction to the experimental crystal
12 compared to α is probably due to the more isotropic ring like crystal structure giving similar growth in
13 all directions, and hence the growth mechanisms and growth rates are probably similar. This
14 postulation was reinforced by the fact that the nature and strength of the intermolecular interactions at
15 the morphologically important faces of the β structure were found to be relatively similar compared to
16 the interactions at the morphologically important faces of the α form.

17 Overall this paper presents the results of a thorough, holistic analysis and methodology for
18 understanding the interrelationship between the molecular and solid-state polymorphic structures with
19 the morphology and surface chemistry of a crystalline system at the molecular level.

20 **Acknowledgements**

21 The authors gratefully acknowledge the UK's EPSRC for the funding of this research through a joint
22 collaborative Critical Mass project between the Universities of Leeds and Manchester (grant
23 references EP/IO14446/1 and EP/IO13563/1) which forms part of the doctoral studies of one of us
24 (IR). We also gratefully acknowledge the Critical Mass team at the University of Manchester lead by
25 Professors Davey and Schroeder for stimulating discussions that inspired and contributed to the
26 research and ideas presented in this paper. In addition, we gratefully acknowledge Dr D. Toroz

52

1 (University of Leeds) for calculating the atomistic charges and Dr. R. B Hammond (University of
2 Leeds) for his assistance in creating the carboxylic acid H-bonding unit for the dimer attachment
3 energy calculation.
4

5 References

- 6 1. P. York, *International Journal of Pharmaceutics*, 1983, **14**, 1-28.
- 7 2. R. B. Hammond, K. Pencheva and K. J. Roberts, *Crystal Growth & Design*, 2007, **7**, 875-884.
- 8 3. R. B. Hammond, S. Jeck, C. Y. Ma, K. Pencheva, K. J. Roberts and T. Auffret, *Journal of*
9 *Pharmaceutical Sciences*, 2009, **98**, 4589-4602.
- 10 4. V. Ramachandran, D. Murnane, R. B. Hammond, J. Pickering, K. J. Roberts, M. Soufian, B.
11 Forbes, S. Jaffari, G. P. Martin, E. Collins and K. Pencheva, *Molecular Pharmaceutics*, 2014,
12 **12**, 18-33.
- 13 5. R. Docherty, G. Clydesdale, K. J. Roberts and P. Bennema, *J. Phys. D-Appl. Phys.*, 1991, **24**, 89-
14 99.
- 15 6. A. Bravais, *Etudes Crystallographiques*, Gauthiers Villars, Paris, 1886.
- 16 7. J. D. H. Donnay and D. Harker, *American Mineralogist*, 1937, **22**, 446-467.
- 17 8. G. Friedel, *Bulletin De La Societe Francaise De Mineralogie Et De Crystallographie*, 1907, **30**,
18 326.
- 19 9. R. Docherty, K. J. Roberts and E. Dowty, *Computer Physics Communications*, 1988, **51**, 423-
20 430.
- 21 10. R. Docherty and K. J. Roberts, *Journal of Crystal Growth*, 1988, **88**, 159-168.
- 22 11. P. Hartman and W. G. Perdok, *Acta Crystallographica*, 1955, **8**, 49-52.
- 23 12. M. Born, *Atom Theorie des Feste Zlrsfande 2nd Edn*, 1923.
- 24 13. E. Dowty, *American Mineralogist*, 1976, **61**, 448-459.
- 25 14. W. K. Burton, N. Cabrera and F. C. Frank, *Philosophical Transactions of the Royal Society of*
26 *London Series a-Mathematical and Physical Sciences*, 1951, **243**, 299-358.
- 27 15. M. Ohara and R. C. Reid, *Modelling Crystal Growth Rates*, 1974.
- 28 16. P. Hartman and P. Bennema, *Journal of Crystal Growth*, 1980, **49**, 145-156.
- 29 17. Z. Berkovitch-Yellin, *Journal of the American Chemical Society*, 1985, **107**, 8239-8253.
- 30 18. G. Clydesdale, R. Docherty and K. J. Roberts, *Computer Physics Communications*, 1991, **64**,
31 311-328.
- 32 19. G. Clydesdale, K. J. Roberts and E. M. Walker, *The crystal habit of molecular materials: A*
33 *structural perspective*, G Clydesdale, K J Roberts and E M Walker, In "Molecular Solid State:
34 *Syntheses, Structure, Reactions, Applications*", 1996.
- 35 20. M. C. Etter, J. C. Macdonald and J. Bernstein, *Acta Crystallographica Section B-Structural*
36 *Science*, 1990, **46**, 256-262.
- 37 21. M. C. Etter, *Accounts of Chemical Research*, 1990, **23**, 120-126.
- 38 22. J. Bernstein, *Polymorphism in Molecular Crystals*, Oxford University Press, USA, 2002.
- 39 23. G. Desiraju, J. J. Vittal and A. Ramanan, *Crystal Engineering: The Design of Organic Solids*,
40 Elsevier, 1989.
- 41 24. G. R. Desiraju, *Angewandte Chemie International Edition in English*, 1995, **34**, 2311-2327.
- 42 25. Q. Wang, D. B. Sheen, E. E. A. Shepherd, J. N. Sherwood, G. S. Simpson and R. B. Hammond,
43 *Journal of Crystal Growth*, 1997, **181**, 418-426.
- 44 26. G. Clydesdale, K. J. Roberts, G. B. Telfer, V. R. Saunders, D. Pugh, R. A. Jackson and P.
45 Meenan, *The Journal of Physical Chemistry B*, 1998, **102**, 7044-7049.

- 1 27. G. Clydesdale, K. J. Roberts, G. B. Telfer and D. J. W. Grant, *Journal of Pharmaceutical*
2 *Sciences*, 1997, **86**, 135-141.
- 3 28. D. E. Williams, *Journal of Chemical Physics*, 1966, **45**, 3770-&.
- 4 29. F. A. Momany, L. M. Carruthers, R. F. McGuire and H. A. Scheraga, *The Journal of Physical*
5 *Chemistry*, 1974, **78**, 1595-1620.
- 6 30. G. Nemethy, M. S. Pottle and H. A. Scheraga, *The Journal of Physical Chemistry*, 1983, **87**,
7 1883-1887.
- 8 31. S. L. Mayo, B. D. Olafson and W. A. Goddard, *Journal of Physical Chemistry*, 1990, **94**, 8897-
9 8909.
- 10 32. A. T. Hagler, S. Lifson and P. Dauber, *Journal of the American Chemical Society*, 1979, **101**,
11 5122-5130.
- 12 33. S. Lifson, A. T. Hagler and P. Dauber, *Journal of the American Chemical Society*, 1979, **101**,
13 5111-5121.
- 14 34. S. L. Price, M. Leslie, G. W. A. Welch, M. Habgood, L. S. Price, P. G. Karamertzanis and G. M.
15 Day, *Physical Chemistry Chemical Physics*, 2010, **12**, 8478-8490.
- 16 35. J. D. Gale, *J. Chem. Soc.-Faraday Trans.*, 1997, **93**, 629-637.
- 17 36. J. D. Gale and N. J. Henson, *J. Chem. Soc.-Faraday Trans.*, 1994, **90**, 3175-3179.
- 18 37. R. B. Hammond, K. Pencheva, V. Ramachandran and K. J. Roberts, *Crystal Growth & Design*,
19 2007, **7**, 1571-1574.
- 20 38. M. K. Singh and A. Banerjee, *Crystal Growth & Design*, 2013, **13**, 2413-2425.
- 21 39. J. Chen and B. L. Trout, *Crystal Growth & Design*, 2010, **10**, 4379-4388.
- 22 40. D. Winn and M. F. Doherty, *Aiche Journal*, 1998, **44**, 2501-2514.
- 23 41. S. Gnanasambandam and R. Rajagopalan, *CrystEngComm*, 2010, **12**, 1740-1749.
- 24 42. C. Schmidt and J. Ulrich, *Chemical Engineering & Technology*, 2012, **35**, 1009-1012.
- 25 43. C. Schmidt and J. Ulrich, *Chemical Engineering & Technology*, 2011, **34**, 563-570.
- 26 44. C. Cambridge Crystallographic Data, *Cambridge Structural Database*, 1965.
- 27 45. W. R. Busing, *Acta Crystallographica Section A*, 1983, **39**, 340-347.
- 28 46. S. Athimoolam and S. Natarajan, *Acta Crystallographica Section C-Crystal Structure*
29 *Communications*, 2007, **63**, O514-O517.
- 30 47. S. Gracin and A. Fischer, *Acta Crystallographica Section E-Structure Reports Online*, 2005, **61**,
31 O1242-O1244.
- 32 48. R. Benali-Cherif, R. Takouachet, E.-E. Bendeif and N. Benali-Cherif, *Acta Crystallographica*
33 *Section C*, 2014, **70**, 323-325.
- 34 49. R. A. Sullivan and R. J. Davey, *CrystEngComm* 2015, **17**, 1015-1023.
- 35 50. M. A. Lovette and M. F. Doherty, *Crystal Growth & Design*, 2013, **13**, 3341-3352.
- 36 51. N. Panina, R. van de Ven, F. F. B. J. Janssen, H. Meekes, E. Vlieg and G. Deroover, *Crystal*
37 *Growth & Design*, 2009, **9**, 840-847.
- 38 52. A. S. Inc, San Diego, 5.5 edn., 2011.
- 39 53. I. J. Bruno, J. C. Cole, P. R. Edgington, M. Kessler, C. F. Macrae, P. McCabe, J. Pearson and R.
40 Taylor, *Acta Crystallographica Section B-Structural Science*, 2002, **58**, 389-397.
- 41 54. G. Clydesdale, K. J. Roberts and R. Docherty, *Journal of Crystal Growth*, 1996, **166**, 78-83.
- 42 55. R. B. Hammond, K. J. Roberts, E. D. L. Smith and R. Docherty, *The Journal of Physical*
43 *Chemistry B*, 1999, **103**, 7762-7770.
- 44 56. D. Toroz, I. Rosbottom, T. Turner, D. M. C. Corzo, R. B. Hammond, X. Lai and K. J. Roberts,
45 *Faraday Discussions (Accepted)*, 2015.
- 46 57. M. J. Frisch, G. W. Trucks, H. B. Schlegel, G. E. Scuseria, M. A. Robb, J. R. Cheeseman, G.
47 Scalmani, V. Barone, B. Mennucci, G. A. Petersson, H. Nakatsuji, M. Caricato, X. Li, H. P.
48 Hratchian, A. F. Izmaylov, J. Bloino, G. Zheng, J. L. Sonnenberg, M. Hada, M. Ehara, K. Toyota,
49 R. Fukuda, J. Hasegawa, M. Ishida, T. Nakajima, Y. Honda, O. Kitao, H. Nakai, T. Vreven, J. A.
50 Montgomery Jr., J. E. Peralta, F. Ogliaro, M. J. Bearpark, J. Heyd, E. N. Brothers, K. N. Kudin,
51 V. N. Staroverov, R. Kobayashi, J. Normand, K. Raghavachari, A. P. Rendell, J. C. Burant, S. S.

54

- 1 Iyengar, J. Tomasi, M. Cossi, N. Rega, N. J. Millam, M. Klene, J. E. Knox, J. B. Cross, V. Bakken,
2 C. Adamo, J. Jaramillo, R. Gomperts, R. E. Stratmann, O. Yazyev, A. J. Austin, R. Cammi, C.
3 Pomelli, J. W. Ochterski, R. L. Martin, K. Morokuma, V. G. Zakrzewski, G. A. Voth, P. Salvador,
4 J. J. Dannenberg, S. Dapprich, A. D. Daniels, Ö. Farkas, J. B. Foresman, J. V. Ortiz, J. Cioslowski
5 and D. J. Fox, Gaussian, Inc., Wallingford, CT, USA, 2009.
- 6 58. E. Dowty, *Am. mineral*, 1980, **65**, 465-472.
- 7 59. H. J. Human, J. P. Van Der Eerden, L. A. M. J. Jetten and J. G. M. Odekerken, *Journal of Crystal*
8 *Growth*, 1981, **51**, 589-600.
- 9 60. L. A. M. J. Jetten, H. J. Human, P. Bennema and J. P. Van Der Eerden, *Journal of Crystal*
10 *Growth*, 1984, **68**, 503-516.
- 11 61. J. S. Stevens, C. R. Seabourne, C. Jaye, D. A. Fischer, A. J. Scott and S. L. M. Schroeder, *Journal*
12 *of Physical Chemistry B (Early View)*, 2014.
- 13 62. M. Nabavian, R. Sabbah, R. Chastel and M. Laffitte, *Journal De Chimie Physique Et De*
14 *Physico-Chimie Biologique*, 1977, **74**, 115-126.
- 15 63. C. G. de Kruif, J. Voogd and J. C. A. Offringa, *The Journal of Chemical Thermodynamics*, 1979,
16 **11**, 651-656.
- 17 64. R. A. Sullivan and R. J. Davey, *CrystEngComm*, 2015.

18

19

CONFIDENTIAL

CrystEngComm Accepted Manuscript